Physics-Based Hot-Carrier Degradation Models

S.E. Tyaginov*, I.A. Starkov°, H. Enichlmair†, J.M. Park†, Ch. Jungemann‡, and T. Grasser*

* Institute for Microelectronics, TU Wien, Wien, Austria

° Christian Doppler Laboratory for Reliability Issues in Microelectronics at the Institute for Microelectronics, TU Wien, Wien, Austria

† Process Development and Implementation Department, Austriamicrosystems AG, Unterpremstätten, Austia

‡ Institute for Microelectronics and Circuit Theory, Bundeswehr University, München, Germany

Abstract

We present a thorough analysis of physics-based hot-carrier degradation (HCD) models. We discuss the main features of HCD such as its strong localization at the drain side of the device, the weakening of the degradation at higher temperatures, and the change of the worst-case condition in small devices. The first feature is related to "hot" carriers, while the second is controlled by the fraction of "colder" particles. The latter feature is related to the change of the silicon-hydrogen bond-breakage mechanism from the single- to multiple-carrier process. All these findings suggest that the interface state creation process is controlled by the manner how the carriers are distributed over energy, that is, by the carrier energy distribution function. We distinguish between three main aspects of the physical picture behind hot-carrier degradation: carrier transport, microscopic mechanisms of defect creation and simulation of degraded devices. Therefore, we analyze and classify the existing HCD models in this context. Finally we present our hot-carrier degradation model based on a thorough evaluation of this distribution function by means of a full-band Monte-Carlo device simulator. Our approach tries to address the whole hierarchy of physical phenomena in order to capture all the essential aspects of hot-carrier degradation.

Introduction

Hot-carrier degradation (HCD) is associated with the build-up of defects at or near the silicon/silicon dioxide interface of an MOS transistor. The degradation is due to the bombardment of the interface by carriers which have gained sufficiently high energy and are thus called "hot" carriers, see [1–3] and references therein. The interface states that are created by this process are characterized by a density N_{it}. They are able to capture electrons/holes and, hence, become charged. The density N_{it} is a distributed quantity, that is, varies with the coordinate along the Si/SiO_2 interface as well as in energy. These additional charges introduced into the system are distributed along the channel and perturb

the electrostatics of the device resulting for instance in a shift of the threshold voltage. Furthermore, they act as additional scattering centers, thereby degrading the mobility and, as a result, the transconductance G_{m} and linear drain current I_{dlin}.

Several hot-carrier degradation mechanisms have been suggested in the literature: channel hot-carrier, drain avalanche hot-carrier, secondary generated hot-carrier, substrate hot-carrier, and Fowler-Nordheim and direct tunneling injection, e.g.[1, 4, 5]. The first mechanism is directly linked to the electric field in the channel of Field-Effect-Transistor (MOSFET) which accelerates carriers. Particles with sufficiently high energy, whereby "sufficiently" depends on a concrete HCD model and may mean energy required to overcome the potential barrier at the interface or trigger the Si-H bond rupture, are called "hot". The drain avalanche and secondary generated hot-carrier mechanisms assume a cascade of impact ionization events caused by a solitary hot carrier, which leads to avalanche generation of electron-hole pairs. Under the substrate hot-carrier mode a uniform injection from the channel-substrate p-n junction occurs; this mode has been actively used in pioneering works devoted to hot-carrier reliability [5]. As for the Fowler-Nordheim and direct tunneling mechanisms, carriers are injected either into the SiO_2 conduction band through the triangular potential barrier (Fowler-Nordheim regime) or to the channel overcoming a trapezoidal barrier (direct tunneling). In modern ultra-scaled devices and/or in high-voltage transistors only the channel hot-carrier regime is relevant and drain avalanche and secondary generated hot carriers are considered as a part of the channel hot-carrier degradation phenomenon. Therefore, further in the text we mean just the channel hot-carrier mode when referring to "hot-carrier degradation".

The first successful attempt to HCD modeling was the so-called "lucky-electron" model proposed by Hu [6, 7]. This concept is based on the following assumptions: (i) an electron characterized by an energy high enough to overcome the potential barrier at the interface (ii) impinges onto the interface without collision, that is, without energy loss and (iii) without being scattered back into the channel and being emitted into the SiO_2 conduction band thereby producing a defect. The "lucky electron" model claims that the threshold of HCD is 3.7 eV, however, hot-carrier stresses performed at $V_{\mathrm{ds}} < 3$ V demonstrated that device aging can also occur at lower voltages [8]. As a consequence, this approach fails for short-channel devices. However, due to its simplicity, the model still remains one of the most popular approaches.

An empirical extension of the "lucky electron" model was proposed by Takeda and Suzuki [9, 10]. This simple time dependent model expresses the transconductance degradation ΔG_{m} and/or threshold voltage shift ΔV_{th} by a time power law t^n. The exponent and proportionality coefficients are fitting parameters adjusted independently for a particular device architecture. The advantage of such an approach is that it allows easy extrapolation the device life-time from accelerated hot-carrier stress conditions to real operation biases. However, the applicability of the model is rather limited as demonstrated by investigations employing lightly doped drain structures where the saturation of degradation after a certain value has been observed ([11] and references therein). Although inaccurate for describing hot-carrier degradation, the Takeda model inspired a number of fitting models. These models try to represent device parameter degradation employing some combinations of time exponents. Among them are the Goo model based

on the "lucky electron" concept, which can capture saturation of degradation [11], the Dreesen model [12, 13], which follows the same strategy but was adapted for lightly doped drain MOSFETs and is able to successfully represent the I_{dlin} degradation in the range of ΔI_{dlin}=0.02%...10%.

Other extensions of the Hu concept have been proposed by Woltjer [14, 15] and by Mistry *et al.* [16, 17]. In contrast to the "lucky electron" model, which deals with interface trap generation under maximum substrate current conditions but fails at other stress conditions, the Woltjer model considers the oxide field as crucial for the creation of interface states. As a result, a field-driven correction is incorporated into the "lucky electron" model. This extension allows description of the degradation behavior of devices with various dimensions and oxide thicknesses. Mistry and co-workers reported that a single degradation mechanism is not sufficient for proper degradation modeling and three different modes of damage were proposed: at low V_{gs} creation of interface states and oxide neutral electron traps occurs while for mid and high V_{gs} only interface state build-up and oxide electron traps, respectively, contribute. All of them are present during DC-stress and each of them can dominate the AC-stress life-time [17]. However, the life-times predicted by this model were rather inaccurate and thus only of limited applicability. Moreover, the general shortcoming of these approaches is that starting from a certain node and beyond, the field-driven paradigm and related modeling approaches, such as extensions of the "lucky electron" model should be substituted by energy-driven concepts [8, 18, 19].

The idea that two (or several) competing degradation mechanism are required to describe the overall degradation has been further extended by Moens *et al.* in order to capture degradation in LDMOS transistors [20–23]. In a series of papers Moens demonstrated that for high-voltage devices one should consider defect build-up in different transistor sections, namely in the channel, accumulation, and bird's beak regions. As a result, different components of the damage are characterized by different time exponents, which explains the different slopes of parameter degradation. The dynamic behavior was reported to be determined by hole trapping/detrapping processes [20, 22].

All models described above have been developed for the description of HCD observed in a particular class of devices. As such, they are empirical or at the best phenomenological. But a proper description of HCD may only be possible when the physical picture is accurately understood and captured by the model. There are five main physics-based concepts for hot-carrier degradation modeling elaborated so far:

- the approach presented by Hess and co-authors [24, 25];
- the empirical extension of the Hess model to make it suitable for TCAD device simulators by development in the work of Penzin *et al.* [26];
- the extension of the reaction-diffusion framework proposed by Alam [27, 28];
- the energy-driven paradigm by Rauch and LaRosa [2, 29];
- the Bravaix model based on the Hess approach [30, 31].

The most important breakthrough in HCD modeling is due to Hess who introduced the interplay between a single- and a multiple-carrier mechanism for Si-H bond-breakage. Since these mechanisms are related to the fractions of "hot" and "colder" carriers, the idea that the matter is controlled by the carrier energy distribution function (DF) was first acknowledged [32]. Notwithstanding the fact that the model is able to explain such a crucial feature of HCD such as the hydrogen/deuterium isotope effect [33], the link between the device microscopic picture of the defect build-up and degradation of device characteristics is missing. An attempt of linking these levels has been undertaken in the successor of the Hess approach, in the Penzin model [26] presenting, in fact, a phenomenological approach for HCD modeling. Another approach is the extension of the reaction-diffusion framework of the negative bias temperature instability (NBTI) in order to capture HCD [27, 28]. This implies, however, that once stress is removed, full recovery should be observable within reasonable times. In reality, the recovery of HCD is very slow, thus suggesting that HCD is a reaction-limited process [34]. One more strategy for HCD modeling proposed by Rauch and LaRosa is called "energy-driven paradigm" [2, 29]. For channel lengths less than 180 nm, HCD was shown to be controlled by the single "knee" energy. This energy is related to the stress bias. Therefore, instead of operating with coordinate-dependent quantities (electric field, dynamic temperature, DF, etc) only a single bias-dependent parameter is considered. A combination of the Hess and Rauch approaches was proposed by Bravaix *et al.* [30, 31]. In this concept the interaction between the single- and multiple-carrier mechanisms for Si-H bond-breakage has been considered. However, crucial point is that the information about the carrier DF is substituted by some empirical factors. In spite of a certain success of all these approaches the main problem is that they capture just a fragment of the whole HCD mosaic. Therefore, the whole hierarchical ladder connecting the microscopic level of defect creation and the device simulation level is still not fully understood.

To summarize, over the last decades hot-carrier degradation modeling has evolved from simple empirical models to a more detailed understanding of the microscopic physics involving single- and multiple-particle processes (SP- and MP-mechanisms). A detailed description of the physics requires knowledge of the carrier energy distribution function (DF) which can only be obtained from a solution of the Boltzmann transport equation. Most models in use today employ simplified solutions based on the average energy or, even more dramatic, the electric field, while in the ultimate simplification it is tried to capture the physics using closed analytic expressions. Although computationally more efficient, these approaches are inevitably inaccurate, even though their limitations might not be that obvious when a limited range of bias conditions, temperatures, and channel-lengths is investigated. Therefore, after describing the main features of hot-carrier degradation, we proceed to the detailed analysis of the existing physics-based HCD models finishing with the presentation and validation of a detailed model.

Characteristic Features of Hot-Carrier Degradation

Although the detrimental phenomenon of hot-carrier degradation has been known for more than four decades, it remains one of the most crucial concerns in transistor reliability. Since during this period of time several generations of Metal-Oxide-Semiconductor

MOSFETs have been in production, the characteristic features of HCD, their understanding, and the modeling approaches also reflect these trends. For instance, in the eighties, the device dimensions have been reduced rather quickly, accompanied by a slower scaling of the transistor power supply. This tendency led to high electric fields in the MOSFET channel, which accelerated carriers up to energies high enough to directly trigger a Si-H bond-breakage process by a solitary carrier, which then was considered "hot" [1, 7, 9]. Such a situation required specific measures in order to suppress carrier heating. Among them was the demand that the supply voltage should scale faster than device dimensions [35–38] in addition to requirements for doping profiles and device geometry, which for instance resulted in lightly doped drain structures [30, 39].

In particular, even though in the 0.25 μm node hot-carrier degradation could be rather dramatic, its importance was expected to reduce drastically for coming nodes [1]. The physical reason behind this expectation was that the source-drain voltage V_{ds} had already been scaled down to 1 – 1.5 V while the threshold energy required for triggering the Si-H bond dissociation process is about ∼3.0 – 3.5 eV. Therefore, it was expected that the carrier would not be heated up to energies sufficient for the Si-H bond-breakage, resulting in a suppression of HCD. Overall, a complete absence of HCD was expected for extremely-scaled devices [3, 25, 30, 40].

In reality, however, even ultra-scaled modern MOSFETs can show severe HCD [3, 30, 31]. This was first demonstrated for gate lengths less than than 0.2 μm and supply voltages below 1.0 V by Mizuno *et al.* [41]. The authors related this finding to an energy exchange mechanism populating the "hot" fraction of carrier ensemble. energies substantially higher than the lattice temperature. Possible mechanisms responsible for such an energy gain include impact ionization [42], Auger recombination [43], electron-phonon [44], and electron-electron scattering [18, 19, 45].

Note that electron-electron scattering is of particular importance for nano-scale devices [3, 30]. Particularly for these devices the situation is even more complicated because the dominant mechanism for Si-H bond-breakage changes from a single-carrier to a multiple-carrier mechanism [3, 25, 30, 40]. For example, in a long-channel or high-voltage device carriers striking the interface are already rather hot and are able to trigger silicon-hydrogen bond rupture by a single collision, which is referred to as the *single-carrier mechanism*. In contrast, such extremely hot carriers do not exist in sufficient quantity in scaled devices. Rather, several particles subsequently bombard a bond, thereby exciting and eventually rupture it, which is referred to as the *multiple-carrier process*. However, these two scenarios are just limiting cases and in a particular device geometry under certain operating/stress conditions a superposition of these two mechanisms has to be expected [46, 47].

The most important consequence of the interplay between single- and multiple-carrier processes is the change of the worst-case condition of hot-carrier degradation: traditionally, the worst-case of HCD occurred at $V_{\mathrm{gs}} = (0.4-0.5)V_{\mathrm{ds}}$, corresponding to the maximal substrate current or – in other words – to the largest impact ionization rate [8, 48–50]. However, this is not always the case even for long-channel devices; for example, in high-voltage p-MOSFETs the worst-case conditions are observed at the maximum gate current and no empirical law exists for this case [51–53]. This regime corresponds to the situa-

tion where the average carrier energy is maximal, that is, the carrier ensemble includes a substantial fraction of particles with energies high enough to induce the bond dissociation following a single impact.

In contrast, in scaled devices the operating voltages are such that a single carrier is unlikely to reach energies sufficiently large to trigger an SP-process. The process of energy interchange between carriers is of a stochastic nature and therefore one may expect that a certain fraction of particles — however small — may still obtain a relatively large energy. Still, although particles able to launch the SP-mechanism are in principle present, their relative number is rather small and, hence, the MP-process becomes dominant [40, 54]. Contrary to the SP-mechanism, the individual carriers contributing to the MP-mechanism require only a relatively low energy. However, a large number of those carriers is needed. Thus, the carrier flux rather than the single-carrier energy becomes important in this case. The maximum carrier flux is obtained at $V_{\rm ds} = V_{\rm gs}$ for both scaled n- and p-MOSFETs [55–58], which now becomes the region of maximum HCD.

As a final note we remark that even in the case of ultra-short devices a certain fraction of "hot" carriers exists because the high-energy tail of the carrier distribution function is populated for instance by the electron-electron scattering process [2, 3]. Therefore, the SP-mechanism will still contribute in these devices. Also, thermalized, that is, "cold", particles still exist even in the case of high-voltage devices, thereby also leading to HCD by the MP-process. To conclude, in a real device under real operating/stress conditions, the interplay between the SP- and MP-modes of bond-breakage has to be considered and is controlled by the way carriers are distributed over energy, that is, by the carrier DF.

Another characteristic feature of HCD is its strong localization near the pinch-off region (or the drain end of the gate), just near the area where the electric field peaks [1, 3, 59–63]. Such a peculiarity is again related to carriers heating up to energies required to launch the bond-breakage process. Since the driving force of this acceleration is the electric field, for the sake of simplicity it is often assumed that the maximum of the interface state generation rate just corresponds to the electric field peak. However, it has been long understood that the DF can follow changes in the electric field only with a certain delay [64]. Therefore, in order to improve over the electric field approximation, such quantities as the carrier temperature have been used to estimate the location of the maximum damage. However, as it was demonstrated for instance in [65, 66], the maxima of different quantities are observed at different positions and therefore the $N_{\rm it}$ peak never directly coincides with that of the electric field. Moreover, Zaka *et al.* showed that different simplified treatments of carrier transport employing the drift-diffusion, energy-transport and spherical harmonics expansion methods (keeping only the $0^{\rm th}$ and $1^{\rm st}$ order polynomials) lead to spurious description of hot-carrier injection [67]. As a result, the spherical harmonics expansion method for Boltzmann transport equation solution with a higher expansion number of the stochastic Monte-Carlo based solver have to be used. This finding is very important because the Si-H bond-breakage process is described by an energy-dependent reaction cross section [30, 68, 69]. Hence, it is important to know the magnitude of the carrier fraction which corresponds to the given energy.

To make the picture complete one should pay attention to the temperature behavior of HCD. Contrary to NBTI, which is made more severe at higher temperatures (see [70, 71]),

hot-carrier induced damage usually becomes less pronounced at elevated temperatures [72–77]. Note that this traditional tendency is typical only for (relatively) long-channel devices while for ultra-scaled MOSFETs HCD becomes more significant at higher temperatures due to the dominant role of electron-electron scattering and its impact on the carrier distribution function [3, 78–80].

To summarize, the essential features of hot-carrier induced degradation unequivocally demonstrate that the matter is controlled by the carrier distribution function. The DF allows us to judge how efficiently the carriers interact with the bonds or – in other words – how intensive the bond dissociation reactions are. As a result, a comprehensive physics-based HCD model is expected to rely on consistent consideration of the microscopic mechanisms of defect creation and the carrier DF. For the calculation of the carrier distribution function a carrier transport module has to be incorporated into the model.

Hot-Carrier Degradation Models

Hess Model

The main breakthrough in the area of HCD modeling associated with the Hess concept was the introduction of two competing mechanisms for Si-H bond-breakage, namely the single- and multiple-carrier processes, see Fig. 1 [24, 32, 69]. A single-particle process is due to the interaction of a high-energetic solitary carrier with the bond. During this interaction energy is transfered to the bond followed by its dissociation. Due to the large disparity of the electron mass and the mass of hydrogen nucleus, the most probable way to deliver such an energy is via excitation of one of the bonding electrons to an antibonding state. As a consequence, a repulsive force acting on the H atom is induced followed by the release of hydrogen. The desorption rate of this process is [32]:

$$R_{\mathrm{SP}} \sim \int_{E_{\mathrm{th}}}^{\infty} I(E)P(E)\sigma(E)\mathrm{d}E, \tag{1}$$

where $I(E)$ is the flux of carriers with energies in the range of $[E; E + \mathrm{d}E]$, $\sigma(E)$ energy-dependent Keldysh-like reaction cross section, $P(E)$ the desorption probability, while the integration starts from the threshold energy E_{th}.

The first success of the theory was achieved when hydrogen/deuterium desorption induced by subsequent bombardment by several ("cold") carriers from the tip of a scanning tunneling microscope (STM) was investigated on hydrogen- and deuterium-passivated Si surfaces [68, 81–84]. These experiments showed that the D-passivated surfaces are much more resistant with respect to electron bombardment compared to hydrogenated ones. In other words, substantially higher densities of STM currents are required to release the same amount of D atoms vs. H atoms. The difference in depassivation rates (Fig. 2) may be more than two orders of magnitude at high voltages, which gave rise to the name "giant isotope effect". The similarities between the dangling bonds at surfaces and interfaces lead to the application of the theory to H-passivated Si/SiO_2 interfaces subjected to HC stress [54, 85–88].

This giant isotope effect was explained by the concept of multivibrational mode ex-

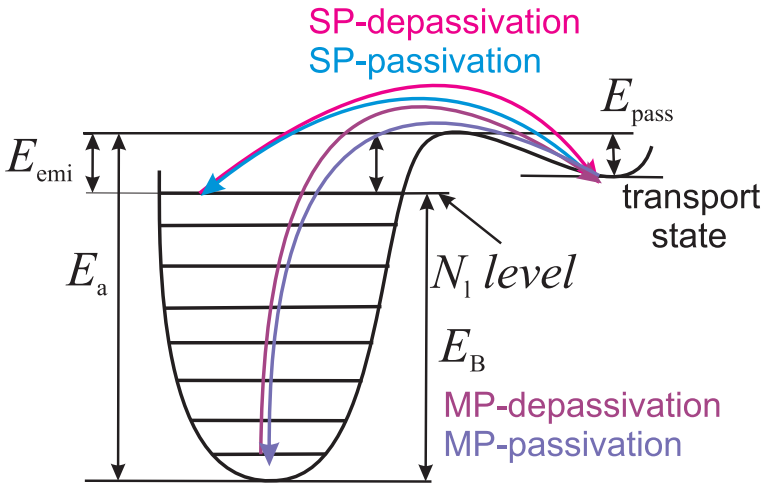

Figure 1: Two competing processes of Si-H bond-breakage: the single- and multiple-carrier mechanisms. The bond is treated as a truncated harmonic oscillator.

citation by linking to the excitation of the phonon modes to a cascade of subsequent bombardments by interfacial carriers. Note that the Si-H bond can relax from an excited state to a lower one and the balance with a reciprocal process has to be considered as well. The bond is treated as a truncated harmonic oscillator (Fig. 1) characterized by a ladder of bonded levels with the last level designated as N_l. The Si-H bond-breakage process is described by the system gradually climbing the ladder of energetic states, a process which is eventually terminated when hydrogen leaves the last bonded level towards the transport state (Fig. 1).

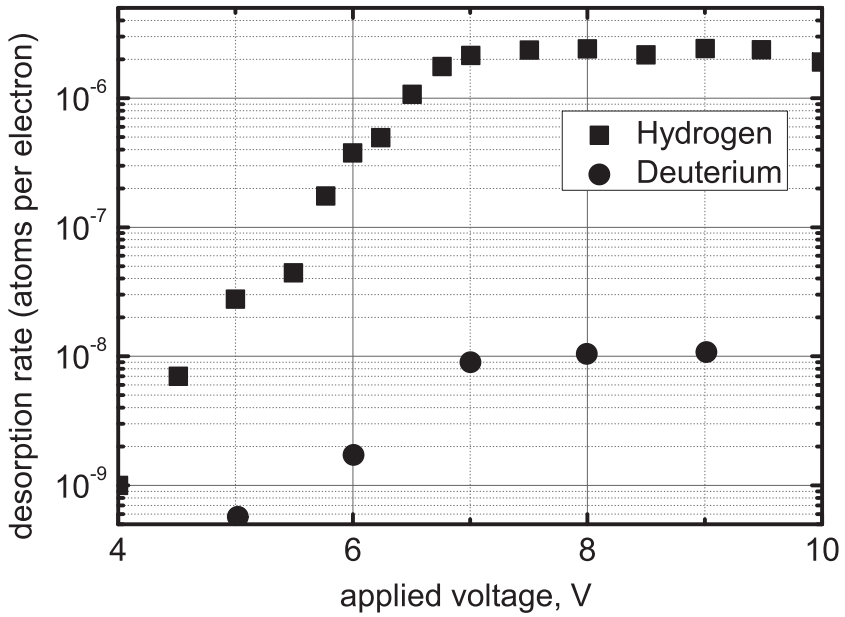

Figure 2: Disparity between H and D desorption rates induced by electrons tunneling from the STM tip on the passivated Si surface (data from [82]).

The reaction rate is defined by the height of the barrier E_{emi} separating the last level N_l and the transport state (Fig. 1). Similarly, the passivation process is related to the

hydrogen jumping into the opposite direction, determined by the barrier height E_{pass}. The corresponding rates ($P_{\mathrm{emi}},\ P_{\mathrm{pass}}$) are assumed to obey an Arrhenius law.

To obtain an expression for the phonon excitation and decay rates P_{u}, P_{d} (Fig. 1), the formalism described in [32, 69] is applied. The electron flux can induce either phonon absorption (that is, bond heating) or phonon emission (related to the multivibrational mode decay). Therefore, these absorption and emission rates, which are just the product of the electron flux and the process capture cross section divided by the phonon occupation number plus one or by the occupation number, respectively. Summarizing all these considerations one obtains the expression for P_{u}, P_{d} [69]:

$$\begin{aligned} P_{\mathrm{d}} &\sim \int_{E_{\mathrm{th}}}^{\infty} I(E)\sigma_{\mathrm{ab}}(E)[1 - f_{\mathrm{ph}}(E - \hbar\omega)]\mathrm{d}E, \\ P_{\mathrm{u}} &\sim \int_{E_{\mathrm{th}}}^{\infty} I(E)\sigma_{\mathrm{emi}}(E)[1 - f_{\mathrm{ph}}(E + \hbar\omega)]\mathrm{d}E, \end{aligned} \tag{2}$$

where $\sigma_{\mathrm{ab}}(E)/\sigma_{\mathrm{emi}}(E)$ are phonon absorption/emission reaction cross sections, $\hbar\omega$ phonon energy and phonon occupation numbers entering the expressions as $f_{\mathrm{ph}}(E)$. Summarizing the findings of (2), one obtains the bond-breakage rate corresponding to the MP-process as

$$R_{\mathrm{MP}} = \left(\frac{E_{\mathrm{B}}}{\hbar\omega} + 1\right)\left[P_{\mathrm{d}} + \exp\left(\frac{-\hbar\omega}{k_{\mathrm{B}}T_{\mathrm{L}}}\right)\right]\left[\frac{P_{\mathrm{u}} + \omega_{\mathrm{e}}}{P_{\mathrm{d}} + \exp(-\hbar\omega/k_{\mathrm{B}}T_{\mathrm{L}})}\right]^{-E_{\mathrm{B}}/\hbar\omega}, \tag{3}$$

with E_{B} being the energy of the last bonded level in the quantum well (Fig. 1) and the phonon reciprocal life-time ω_{e}; k_{B} and T_{L} are the Boltzmann constant and the lattice temperature, respectively.

It is worth emphasizing that the particle flux differential $I(E)$ entering formulae (1,2) assumes that the carrier DF implicitly enters the expression. Thus, one of the main conclusions of the works by the group of Hess is the idea that for a *proper description of HCD, the carrier energy distribution function* is required. Another important achievement of this concept the isotope effect is essentially explained because different energetics of Si-H and Si-D lead to different parameters of the corresponding quantum wells (see Fig. 1), that is, to different positions of the last level E_{B} and phonon life-time τ.

Another characteristic feature of the Hess model is the assumption that the *activation energy* E_{a} for the Si-H bond-breakage rate is statistically distributed, see Fig. 1. This assumption is supported by *ab initio* calculations using density functional theory [69, 89]. As a consequence, the dispersion of E_{a} leads to different power-law slopes during degradation, see Fig. 3 [24, 25, 40]. This is essential as simple first-order kinetics of Si-H bond-breakage with a single-valued activation energy lead to an exponential transition between the bonded and broken states within about a single decade in time. However, experimental observations demonstrate a double-power law of degradation:

$$N_{\mathrm{it}} \sim \frac{p_1}{1 + (t/\tau_1)^{-\alpha_1}} + \frac{p_2}{1 + (t/\tau_2)^{-\alpha_2}}, \tag{4}$$

where τ_1/τ_2 are characteristic times and α_1/α_2 are two different sublinear time slopes ($\sim 1/2$). This time evolution has been explained assuming that two different types of

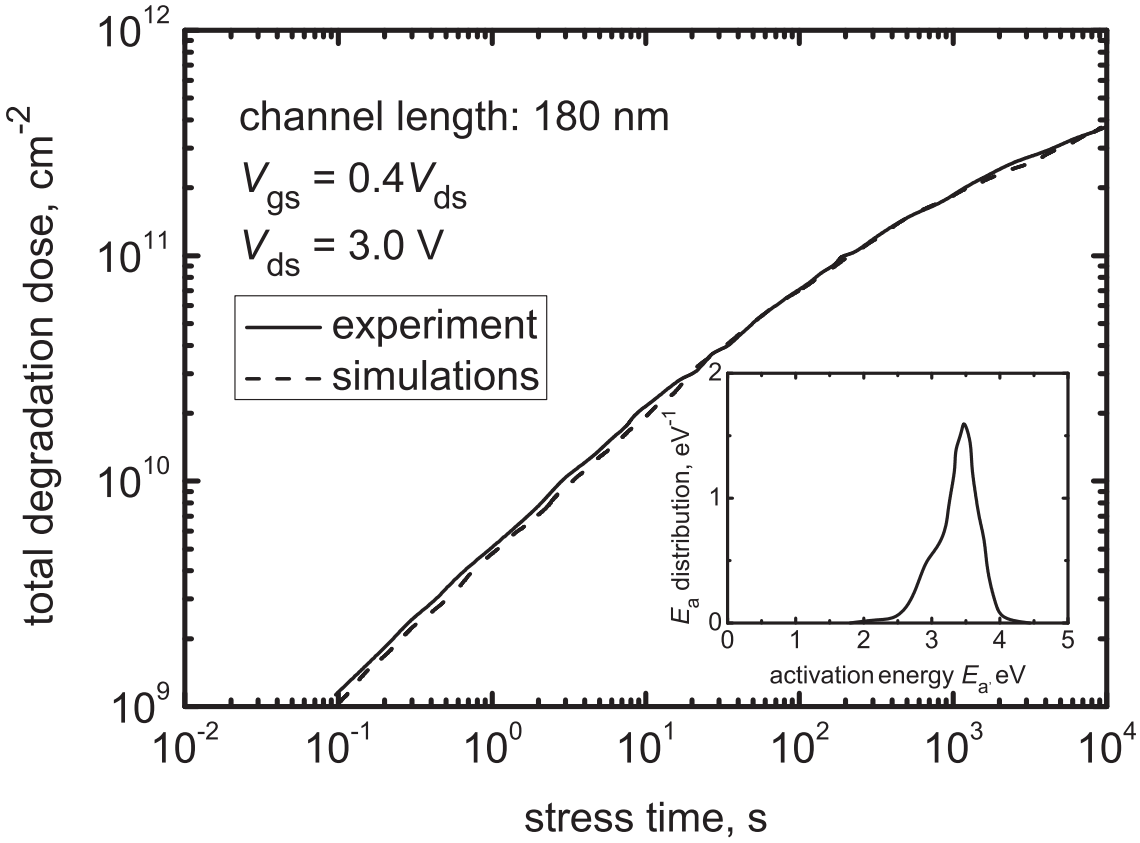

Figure 3: The total degradation dose (cumulative $N_{\rm it}$) as a function of stress time: experiment vs. theory obtained for a 180 nm device under worst-case stress conditions, i.e. $V_{\rm gs} = 0.4V_{\rm ds}$. Inset: distribution of Si-H bond-breakage activation energy. The data are borrowed from [25].

traps (realized with the probabilities p_1 and p_2) contribute to HCD. These traps are similarly distributed and can be fit by the derivative of the Fermi-Dirac function with different mean values $E_{\rm am,1}/E_{\rm am,2}$ and standard deviations $\sigma_{\rm a,1}/\sigma_{\rm a,2}$ [90], see Fig. 3, inset:

$$E_{\rm a,1/2} \propto \frac{1}{\sigma_{\rm a,1/2}} \frac{\exp\left(\dfrac{E_{\rm am,1/2} - E_{\rm a,1/2}}{\sigma_{\rm a,1/2}}\right)}{\left[1 + \exp\left(\dfrac{E_{\rm am,1/2} - E_{\rm a,1/2}}{\sigma_{\rm a,1/2}}\right)\right]^2} \tag{5}$$

Despite the significant progress due to the work of Hess *et al.*, the interface traps are considered on a microscopic level and remain unconnected to the device level. For instance, the device life-time is estimated as the time when the concentration $N_{\rm it}$ reaches a certain level. Also, the degradation of such parameters as transconductance, linear drain current and so forth, is not really addressed. Furthermore, although the necessity of evaluation of the carrier DF is acknowledged, in practice this information has not been incorporated into the approach. As a result, the model operates with some overall $N_{\rm it}$, thereby not considering its distributed nature and that the details in the $N_{\rm it}$ distribution follows the features found in the DF.

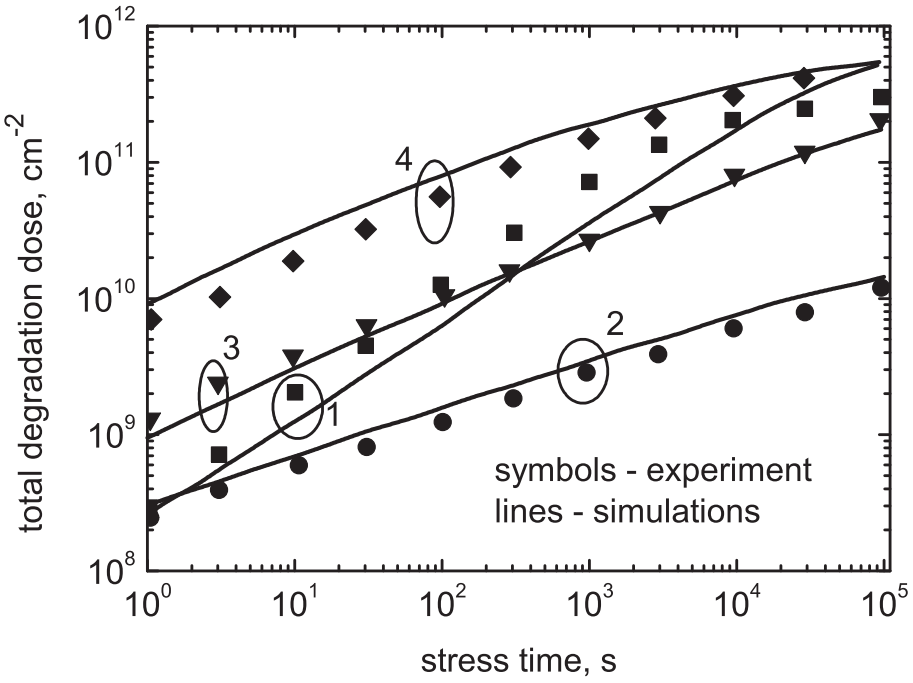

Figure 4: The interface state concentration $N_{\rm it}$, simulation vs. experiment. An n-MOSFET with a gate length of 0.35 μm and an oxide thickness of 6.5 nm was subjected to hot-carrier stress at (1): $V_{\rm gs}$ = -9V, $V_{\rm ds} = V_b = 0$V (V_b is the substrate voltage); (2): $V_{\rm gs} = 12$V, $V_b = 0$V and floating source and drain; (3): $V_{\rm gs} = 1$V, $V_{\rm ds} = 0$V, V_b = -11V; (4): $V_{\rm gs} = 2.5$V, $V_{\rm ds} = 5$V, $V_b = 0$V. Data from [26].

Penzin Model

The Hess model was adapted for TCAD device simulations by Penzin *et al.* [26, 91] by employing phenomenological approximation. The model omits the microscopic level of defect generation (with the interplay of the SP- and MP-mechanisms as the essential attribute) but operates already on the device level. The bond rupture process is described by a kinetic equation for the passivated bond concentration n:

$$\frac{{\rm d}n}{{\rm d}t} = -kn + \gamma(N_0 - n), \tag{6}$$

where k is the forward (depassivation) reaction rate while γ is the backward (passivation) rate and N_0 the total concentration of both "virgin" and broken bonds. The forward reaction rate has the following structure: $k = k_0 \exp(-E_{\rm a}/k_{\rm B}T_{\rm L})k_{\rm H}$ with the attempt frequency k_0 and $k_{\rm H}$ being the hot-carrier acceleration factor. This term is controlled by the "local hot carrier current" [26] $I_{\rm HC}$:

$$k_{\rm H} = 1 + \delta_{HC}|I_{\rm HC}|^{\rho_{HC}}, \tag{7}$$

where $\delta_{\rm HC}$ and $\rho_{\rm HC}$ are fitting parameters.

An important peculiarity of the Penzin approach is that the *activation energy* of bond dissociation *depends on the hydrogen density* and the transversal component of the electric field. The Si/SiO_2 interface (and its vicinity) is considered as a capacitor. The released

hydrogen is assumed to be charged as well as the remaining dangling bonds. As a results, an additional electric field related to these charges is introduced into the system. This field prevents subsequent hydrogen ions from leaving the system and thus the potential barrier separating bonded and transport states is increased:

$$\begin{aligned} E_{\mathrm{a}} &= E_{\mathrm{a}}^{0} + \delta|F|^{\rho} + \beta k_{\mathrm{B}} T_{\mathrm{L}} \ln \frac{N_0 - n}{N_0 - n^{(0)}} \\ \beta &= 1 + \beta_{\perp} F_{\perp}, \end{aligned} \tag{8}$$

with E_{a}^{0} being the activation energy in the absence of mobile H and $n^{(0)}$ the preexisting mobile hydrogen concentration. Since the system is considered as a capacitor, removal of charge from the capacitor is related to an additional energy required to compensate the change of the electric field. This energy is proportional to the capacitor electric field, that is in this case the normal (to the interface) component $F_{\perp}$ entering the expression. Additionally, the external electric field F can stretch or squeeze the bond, thereby changing the activation energy which is controlled by the term $\delta|F|^{\rho}$.

Similarly to the approach of Hess, the model employs a distribution of the activation energy and thus is able to represent the sublinear slope of degradation; Fig. 4 demonstrates a reasonable agreement between experiment and theory. Although the model attempts to capture the carrier transport, this issue still remains vague. The formula 7 includes the acceleration factor related to the *"local hot carrier current" which is the equivocal matter*, i.e. it would be reasonable to define a *criterion to distinguish "hot" and "cold" carriers*. This criterion may be based for instance on the *carrier temperature, which is related to the average energy of the distribution function* (compare with the expressions (1, 2)). As an adjacent problem, the information about the N_{it} profile is hardly achievable. Moreover, in spite of the efforts to link the kinetics of the trap generation and the device characteristics, we are not aware of a rigorous comparision against experimental device characteristics. Instead the soundness of the model is only proven by representing the experimental value of some cumulative N_{it} (Fig. 4), but such a representation has already been obtained within the Hess approach, see Fig. 3.

Reaction-Diffusion Framework

Another approach focused on the physical picture behind hot-carrier degradation was developed by the group of Alam [27, 92]. The assumption was that NBTI and HCD are related to the breakage of silicon-hydrogen bonds, differing only in the driving force triggering this dissociation. Therefore, both phenomena are to be coupled within the same modeling framework. The authors claimed that since NBTI is just the breakage of Si-H bonds followed by hydrogen release and diffusion, NBTI and HCD are to be united within the reaction-diffusion concept.

Experimental observations demonstrated that time signatures of NBTI and HCD have different power-law slopes, i.e. the former one can be approximated by a $t^{1/4}$ law while the latter one better obeys a $t^{1/2}$ dependence, see Fig. 5 and [27, 92]. The reaction-diffusion framework includes the following stages [92, 93]:

1. Creation of interface states via breaking Si-H bonds. This stage is reaction-limited and described by a t^{1} dependence.

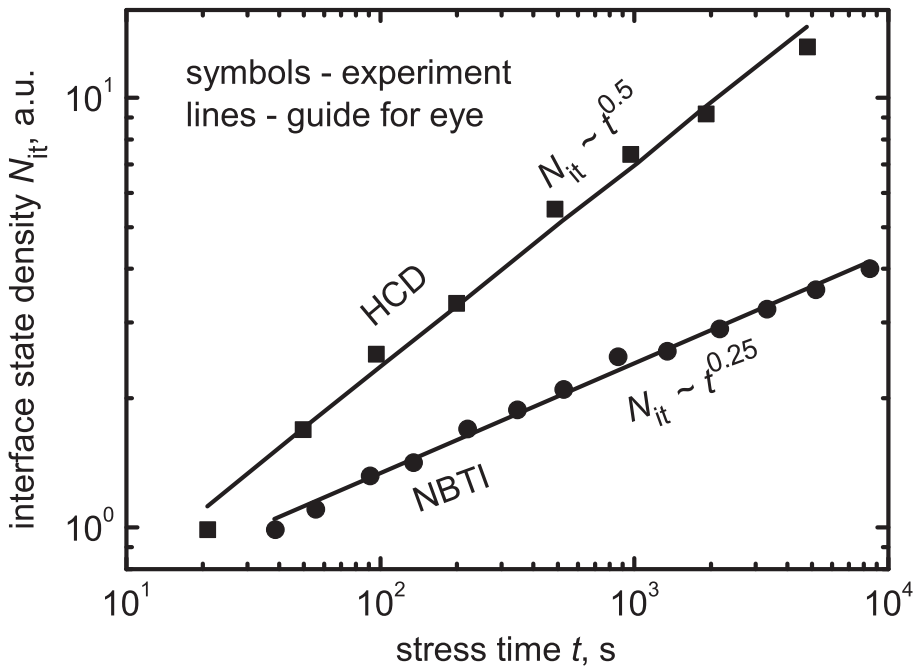

Figure 5: Different time slopes of hot-carrier induced degradation and NBTI. The data are borrowed from [27].

2. Hydrogen diffusion begins to take over with no more interface states created: $N_{\rm it} \sim t^0$.

3. Diffusion-limited phase with $t^{1/4}$ behavior.

4. Hydrogen diffuses away with unlimited diffusion velocity resulting in the 1/2 degradation time slope, i.e. $N_{\rm it} \sim t^{1/2}$.

5. Finally, saturation occurs when all the "virgin" Si-H bonds are depassivated: $N_{\rm it} \sim t^0$.

Therefore, it was assumed that NBTI is diffusion-limited which describes its $t^{1/4}$ behavior while HCD is controlled by the $4^{\rm th}$ phase. However, this scenario presumes that in the case of HCD a transition from $t^{1/4}$ to $t^{1/2}$ is to be observed but the authors of [92] claim that in practice no experimental evidence of such a transition is known. Instead, they suggest that the difference in time slopes is related to the circumstance that NBTI is a 1D problem while HCD is a 2D phenomenon due to the non-uniform $N_{\rm it}$ distribution over the lateral coordinate. Since the Si-H bond-breakage event generates one mobile hydrogen and one interface trap one writes $N_{\rm it} = \int N_{\rm H}(r,t){\rm d}^3r$ ($N_{\rm H}(r,t)$ is the coordinate-dependent hydrogen concentration). The diffusion front moves like $(D_{\rm H}t)^{1/2}$

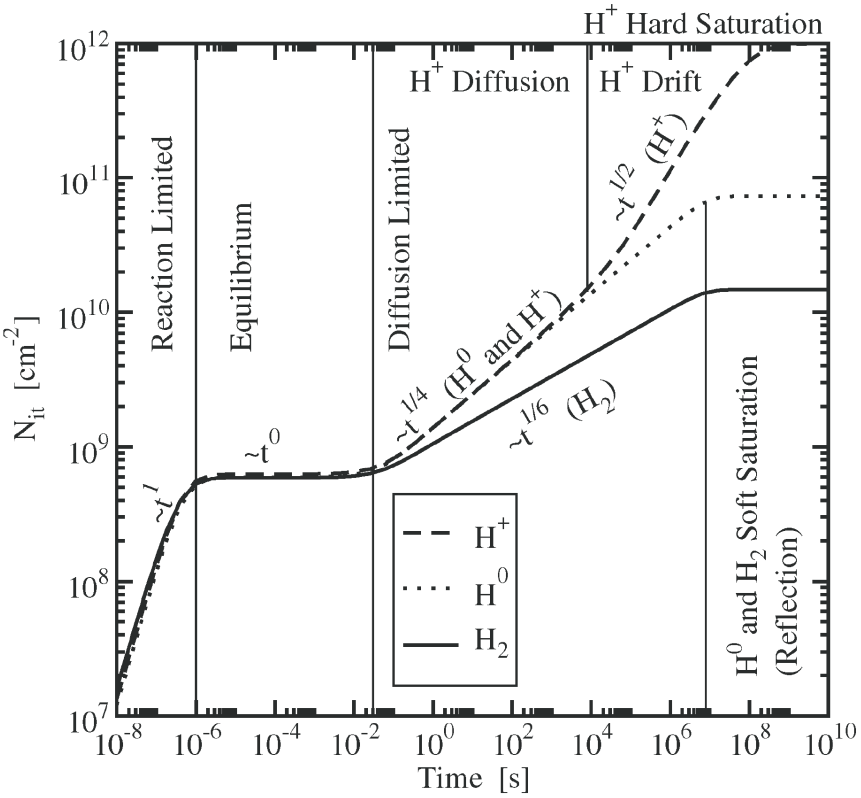

Figure 6: The main phases of the reaction-diffusion model applied to NBTI with different time slopes being marked.

and thus NBTI- and HCD-related $N_{\rm it}$ are:

$$N_{\rm it}^{\rm (NBTI)} = (1/A_{\rm d}) \int_0^{(D_{\rm H}t)^{1/2}} N_{\rm H}^{(0)} \left[1 - r/(D_{\rm H}t)^{1/2}\right] A_{\rm d}{\rm d}r = (1/2) N_{\rm H}^{(0)} (D_{\rm H}t)^{1/2}$$
$$N_{\rm it}^{\rm (HCD)} = \frac{\pi}{2A_{\rm d}} \int_0^{(D_{\rm H}t)^{1/2}} N_{\rm H}^{(0)} \left[1 - r/(D_{\rm H}t)^{1/2}\right] r{\rm d}r = \frac{\pi}{12A_{\rm d}} N_{\rm H}^{(0)} (D_{\rm H}t), \qquad (9)$$

where $D_{\rm H}$ is the hydrogen diffusivity, $A_{\rm d}$ the area of the degraded spot and $N_{\rm H}^{(0)}$ is the H density at the interface. Assuming that $N_{\rm it} N_{\rm H}^{(0)} \sim$ const, one obtains that $N_{\rm it}^{\rm (NBTI)} \sim (D_{\rm H}t)^{1/4}$ and $N_{\rm it}^{\rm (HCD)} \sim (D_{\rm H}t)^{1/2}$.

Despite its ability to explain the different time slopes of NBTI and HCD, this reaction-diffusion model suffers from serious shortcomings. First, within this framework it is assumed that both phenomena are diffusion limited. This implies, however, that once the stress is removed recovery should occur rather quickly. Recent NBTI data suggest, however, that *interface state creation is reaction rather than diffusion limited* [71, 94, 95]. Concerning *HCD*, the *recovery is in general rather weak* if there is any recovery at all. Second, the model does not rely on carrier transport, that is, it does not consider the driving force behind the trap generation. As a consequence, the $N_{\rm it}$ distribution and the localized nature of the damage are not addressed.

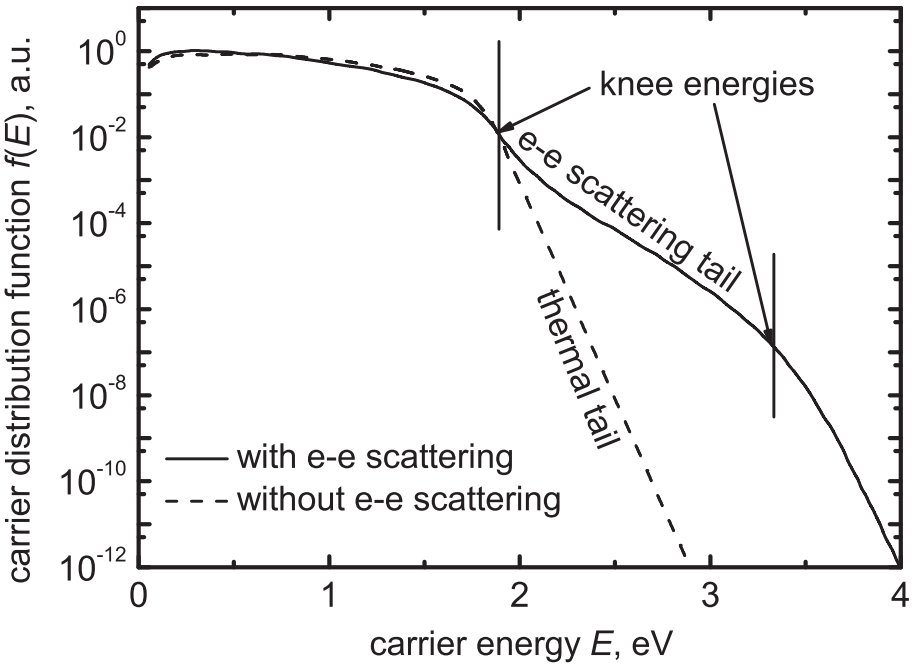

Figure 7: The impact of electron-electron scattering on the shape of the carrier energy distribution function. In the former case an additional hump in the DF high-energy tail appears. Data from [2].

Two main issues associated with the works of Rauch and LaRosa are:

- the increasing impact of electron-electron scattering on HCD at reduced channel lengths [8, 18]
- and the idea that in the case of scaled devices with channel lengths less than 180 nm, the driving force of HCD is the carrier energy rather than the electric field[2, 29, 96].

Electron-electron scattering is of special interest in the case of ultra-scaled MOSFETs because in these devices the supply voltage is rather low and therefore the single-carrier mechanisms of Si-H bond-breakage were expected to be suppressed. This energy exchange mechanism, however, populates the "hot" fraction of the DF and modifies the shape of the DF, that is, results in a pronounced hump in the carrier distribution function, see Fig. 7. Thus, the high-energy tail of the DF can expand deeper into energy than expected from the supply voltage. As a result, the contribution from the SP-mechanism is increased. Additionally, just electron-electron scattering defines the acceleration of HCD at elevated temperatures, which is pronounced in the case of extremely-scaled MOSFETs [3, 78–80].

The energy-driven paradigm presented by Rauch and LaRosa claims that beyond the 180 nm node the driving force of HCD is the energy deposited by carriers, not the maximal electric field in the channel as it was in the "lucky electron model"[7]. Both the impact ionization rate as well as the rate of hot-carrier induced interface state generation is controlled by integrals of the form $\int f(E)S(E)\mathrm{d}E$, where $f(E)$ is the carrier DF and $S(E)$ the reaction cross section; compare this to the formula (1) used previously which has the

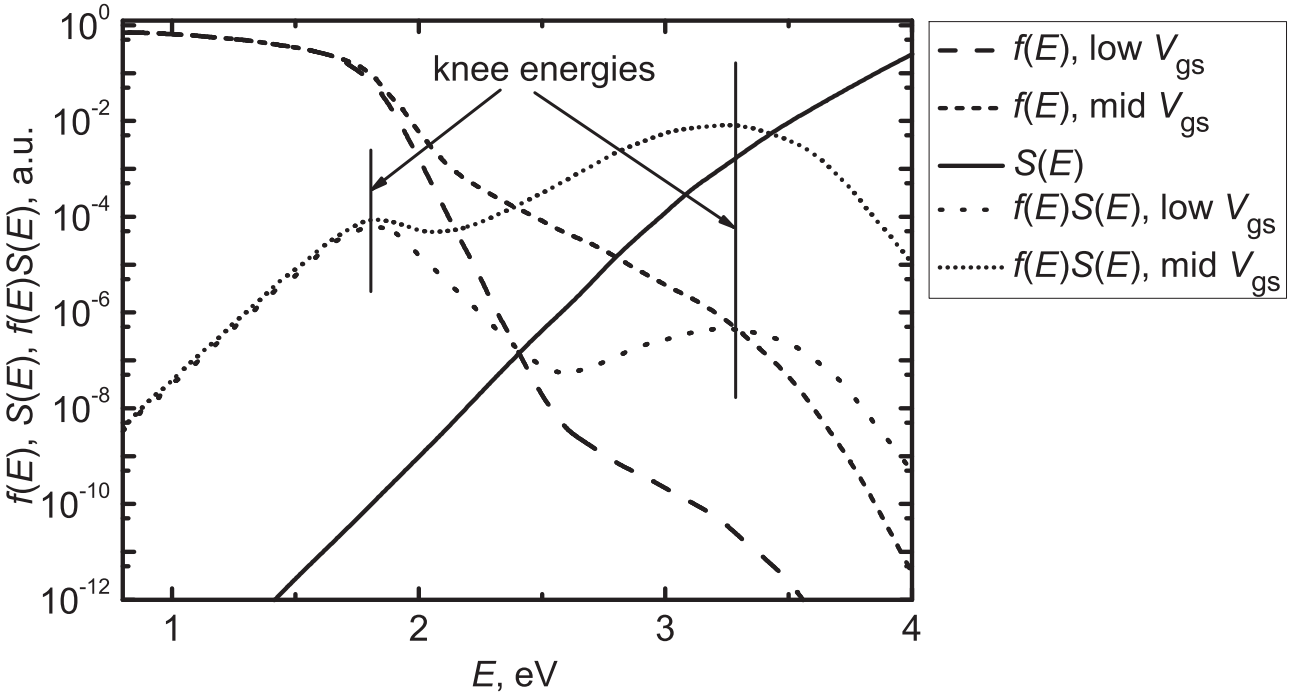

Figure 8: Schematic representation of the energy-driven paradigm. Knee energies shift depending on the applied voltage (the data borrowed from [2]).

same structure. The DF is a strongly decaying function of energy while $S(E)$ grows as a power-law. Hence, this trade-off results in a maximum of the rate pronounced at a certain energy (Fig. 8) determined according to the criterion $\mathrm{d}\ln f/\mathrm{d}E = -\mathrm{d}\ln S/\mathrm{d}E$. This energy E_{knee} is called *"knee" energy* and *is a weak function of the applied bias* V_{ds}. Therefore, if the maximum of the product $f(E)S(E)$ is sufficiently narrow, it can be approximated by a delta-function and instead of integration in the whole energy range one can only calculate the value of the integrand for this energy. To conclude, *the main message of the energy-driven paradigm is that one may avoid time-consuming calculations of the carrier DF* substituting it by the empirical parameter. This parameter is proportional to the reaction rate calculated for $E = E_{\mathrm{knee}}$ which is defined by the bias conditions. This dependence will be discussed in the next subsection devoted to the Bravaix model.

Although this paradigm substantially simplifies the treatment of HCD, it suffers from some shortcomings. Indeed, one can see in Fig. 8 that the maximum is of the integrand $f(E)S(E)$ is not necessarily narrow and in the particular case shown by the authors [2] has a width of 1.5 - 2 eV. Therefore, the concept of a dominant energy sounds doubtful. Furthermore, such a treatment of HCD does not deal with N_{it} as a distributed quantity and thus one of the main features of HCD – its strong localization – is not captured. Finally, as it was in the Hess approach, the device life-time is estimated by the interface state generation rate. However, it would be more reasonable to define it as the time when the degradation of V_{th} or I_{dlin}, etc., has reached a critical value.

Bravaix Model

The model of Bravaix *et al.* inherits the main features of both the Hess and the Rauch/LaRosa approaches: the interplay between single- and multiple-carrier mechanisms as well as the idea that the damage is defined by the carrier DF, which is implemented using Rauch/LaRosa's "fashion", that is, calculations of the DF are substituted by operation/stress condition-related empirical factors.

To describe the MP-process the authors use the formalism of Hess where the Si-H bond is treated as a truncated harmonic oscillator. Following Hess they employ a system of rate equations to describe the kinetics of the oscillator [30, 32]:

$$\begin{aligned}
\frac{\mathrm{d}n_0}{\mathrm{d}t} &= P_\mathrm{d} n_1 - P_\mathrm{u} n_0 \\
\frac{\mathrm{d}n_\mathrm{i}}{\mathrm{d}t} &= P_\mathrm{d}(n_{\mathrm{i}+1} - n_\mathrm{i}) - P_\mathrm{u}(n_\mathrm{i} - n_{\mathrm{i}-1}) \\
\frac{\mathrm{d}n_{N_\mathrm{l}}}{\mathrm{d}t} &= P_\mathrm{u} n_{N_\mathrm{l}-1} - \lambda_\mathrm{emi} N_\mathrm{it}[H^*],
\end{aligned} \tag{10}$$

where $[H^*]$ is the concentration of the mobile hydrogen and n_i is the occupancy of the the i^th oscillator level. In the last equation corresponding to the last bonded level (labeled as N_l, see Fig. 1) the terms representing the passivation (i.e. from the transport to the last bonded state) and transition from the N_l to $N_\mathrm{l} - 1$ state are omitted. The hydrogen released to the transport state is characterized by the rate $\lambda_\mathrm{emi} = \nu_\mathrm{emi}\mathrm{exp}(-E_\mathrm{emi}/k_\mathrm{B}T_\mathrm{L})$ with E_emi being the height of the barrier separating bonded and transport states (see Fig. 1) and ν_emi the attempt frequency.

Similarly to [32], the phonon excitation/decay rates are written in a slightly modified form compared to (2):

$$\begin{aligned}
P_\mathrm{u} &= \int I_\mathrm{d}\sigma \mathrm{d}E_\mathrm{e} + \omega_\mathrm{e}\mathrm{exp}(-\hbar\omega/k_\mathrm{B}T_\mathrm{L}) \\
P_\mathrm{d} &= \int I_\mathrm{d}\sigma \mathrm{d}E_\mathrm{e} + \omega_\mathrm{e},
\end{aligned} \tag{11}$$

with I_d being the source-drain current. Employing the energy-driven paradigm the hot carrier acceleration factor – which is the first terms in (11) – substituted by the empirical factor S_MP:

$$\begin{aligned}
P_\mathrm{u} &= S_\mathrm{MP}(I_\mathrm{e}/e) + \omega_\mathrm{e}\mathrm{exp}(-\hbar\omega/k_\mathrm{B}T_\mathrm{L}) \\
P_\mathrm{d} &= S_\mathrm{MP}(I_\mathrm{e}/e) + \omega_\mathrm{e}.
\end{aligned} \tag{12}$$

The solution of the system (10) for the case of weak bond-breakage rate ($\lambda_\mathrm{emi} t \ll 1$) leads to a square root time dependence of N_it [30]:

$$N_\mathrm{it} = (N_0 \lambda_\mathrm{emi}[P_\mathrm{u}/P_\mathrm{d}]^{N_\mathrm{l}}) t^{1/2}. \tag{13}$$

In addition it was assumed that the bond is predominately situated in the ground state, i.e. $n_0 \approx \sum n_\mathrm{i} \approx N_0$. The MP-related interface state generation rate is:

$$R_\mathrm{MP} \sim N_0 \left[\frac{S_\mathrm{MP}(I_\mathrm{d}/e) + \omega_\mathrm{e}\mathrm{exp}(-\hbar\omega/\mathrm{k_B}T_\mathrm{L})}{S_\mathrm{MP}(I_\mathrm{d}/e) + \omega_\mathrm{e}}\right]^{E_\mathrm{B}/\hbar\omega} \mathrm{exp}(-E_\mathrm{emi}/\mathrm{k_B}T_\mathrm{L}). \tag{14}$$

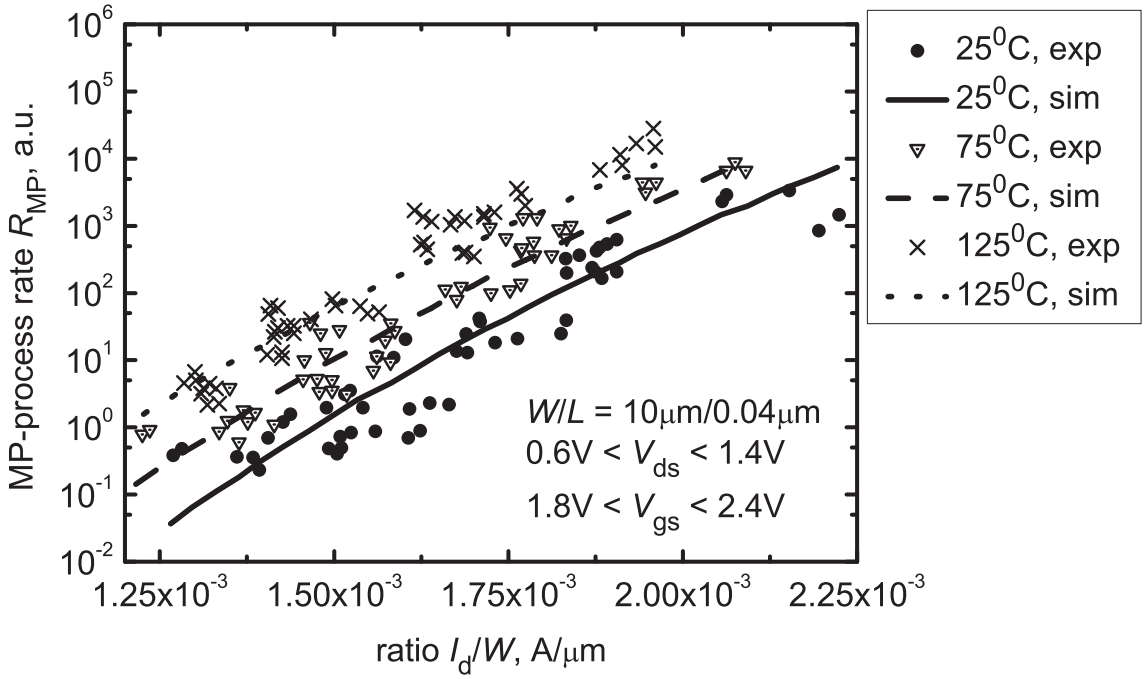

Figure 9: Experimental bond dissociation rate for the MP-process vs. the theoretical one. The information about stress conditions is shown on the canvas. The data are borrowed from [31].

An important question is the choice of quantities (such as $E_{\rm B}$, $E_{\rm emi}$, $\hbar\omega$) defining the energetics of the Si-H bond. In fact, the two main vibrational modes of the Si-H bond are the stretching and bending mode [87] with the main parameters summarized in Table 1 [30]. However, as was previously shown, the experimental data is better fitted by the bending mode and therefore the values corresponding to this mode are employed. The formalism elaborated by Hess and co-authors and refined by Bravaix *et al.* with reasonably chosen simulation parameters allows for perfect representation of the bond dissociation rate by the MP-mechanism, see [31] and the graph from there (Fig. 9).

Table 1: The parameters of the stretching and bending vibrational modes of the Si-H bond.

Parameters	Stretching	Bending
$E_{\rm b}$, eV	2.5	1.5
$\hbar\omega$, eV	0.25	0.075
$w_{\rm e}$, ps^{-1}	1/295	1/10

Furthermore, the SP- and MP-mechanisms for defect creation are considered within Rauch's energy-driven paradigm, that is, are related to the regimes distinguished by Rauch *et al.* [18, 29]:

The regime with low drain current and high carrier energies corresponds to the "hot-carrier" regime where the SP-mechanism plays the dominant role [31]. In this case the "lucky electron" model is valid and the device life-time is:

$$1/\tau_{\rm SP} \sim (I_{\rm d}/W)(I_{\rm s}/I_{\rm d})^m, \tag{15}$$

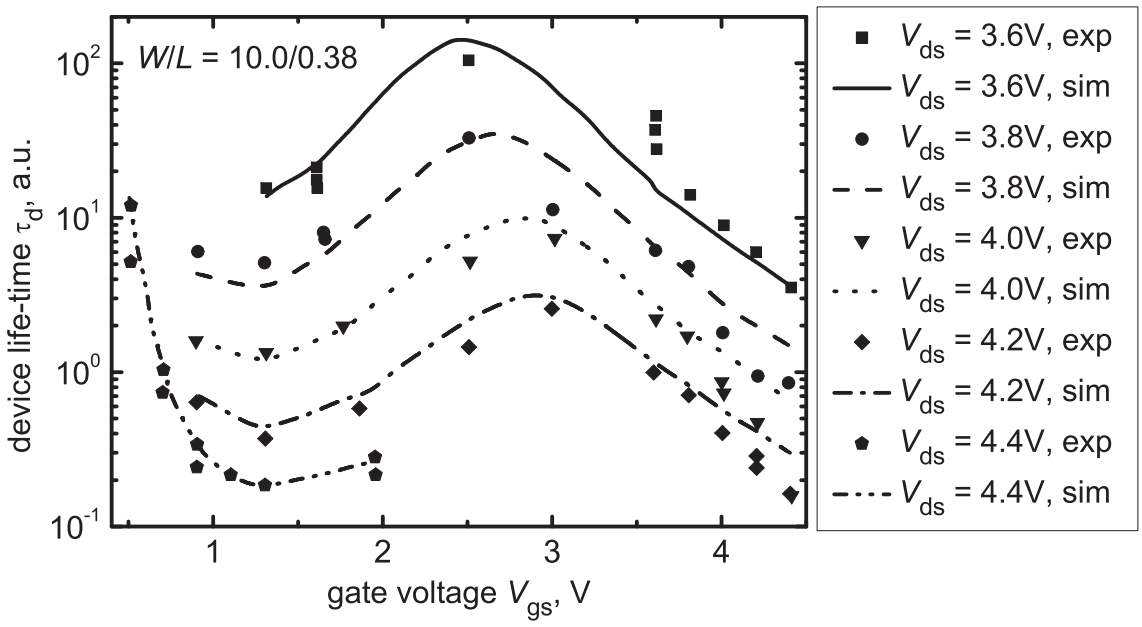

Figure 10: Comparison between the experimental device life-time and that calculated within the Bravaix framework (for devices fabricated in a 65 nm node). The data are taken from [19].

where $I_{\rm s}$ is the substrate current, W the device width and the factor m is the ratio between the powers in the impact ionization and interface state creation cross sections, i.e. $m \cong 11.0/4.0 \approx 2.7$.

Another limiting case corresponds to the high electron flux with low carrier energies. In this situation the MP-process dominates the bond dissociation and the device life-time is $1/R_{\rm MP}$ (14). According to the knee energy concept, $S_{\rm MP} \sim (V_{\rm ds} - \hbar\omega)^{1/2}$, and we have:

$$1/\tau_{\rm MP} \sim [(V_{\rm ds} - \hbar\omega)^{1/2}(I_{\rm s}/W)]^{E_{\rm B}/\hbar\omega}\exp(-E_{\rm emi}/{\rm k_B}T_{\rm L}) \approx [V_{\rm ds}^{1/2}(I_{\rm d}/W)]^{E_{\rm B}/\hbar\omega}. \qquad (16)$$

The intermediate case with moderate drain current and moderate $V_{\rm ds}$ is governed by electron-electron scattering with the corresponding life-time [31]:

$$1/\tau_{\rm EES} \sim (I_{\rm d}/W)^2(I_{\rm s}/I_{\rm d})^m. \qquad (17)$$

This quadratic signature is due to impact ionization which generates electron-hole pairs which are still cold in terms of bond-breakage but being further accelerated by electron-electron scattering up to energies ensuring triggering bond dissociation. Since under real device stress/operation conditions all the modes are present, one writes the device life-time considering these competing mechanisms as

$$1/\tau_{\rm d} = K_{\rm SP}/\tau_{\rm SP} + K_{\rm EES}/\tau_{\rm EES} + K_{\rm MP}/\tau_{\rm MP}, \qquad (18)$$

that is, different contributions are weighted with corresponding probabilities ($K_{\rm SP}$, $K_{\rm EES}$, $K_{\rm MPs}$ which are fitting parameters) and summed. Fig. 10 shows a fit of the model to experimental life-times.

Hot-Carrier Degradation Model Based on the Carrier Distribution Function

We have proposed and verified a more detailed approach for hot-carrier degradation modeling which tries to more accurately capture the physical picture behind this phenomenon [46, 47, 97, 98]. This model incorporates the crucial features of the previous approaches for hot-carrier degradation modeling. But contrary to the previous HCD models we aim at covering and linking all the levels related to this effect, starting from microscopic mechanisms of defect generation and ending at the device level. To be concrete, a physics-based model of HCD may be conditionally separated into three main sub-tasks: the carrier transport module, a module describing the defect build-up during the stress and a module responsible for the simulation of the degraded devices. This concept is sketched in Fig. 11, showing the whole chain of simulation tools employed for the model implementation. Carrier transport is treated with the full-band Monte-Carlo device simulator MONJU [99]. Simultaneously, results obtained with MONJU are verified by the device and circuit simulator developed by our Institute [100]. The drift-diffusion and hydrodynamic schemes implemented into MINIMOS-NT are suitable for carrier transport description in long-channel devices; otherwise MONJU or another Boltzmann transport equation solver is used. The carrier transport module allows us to thoroughly evaluate the carrier energy distribution function for a particular device architecture. The distribution function represents populations of "hot" and "colder" carriers and thus controls the interplay between the SP- and MP-mechanisms.

This DF is then used to calculate the carrier acceleration integral (AI) as a function of the coordinate x along the Si/SiO_2 interface which controls both SP- and MP-mechanisms (the structure is similar to Eq. 2):

$$\begin{aligned} I_{\mathrm{SP}} &= \int\limits_{E_{\mathrm{th,SP}}}^{\infty} f(E)g(E)\sigma_{\mathrm{SP}}(E)v(E)\mathrm{d}E \\ I_{\mathrm{MP}} &= \int\limits_{E_{\mathrm{th,MP}}}^{\infty} f(E)g(E)\sigma_{\mathrm{MP}}(E)v(E)\mathrm{d}E, \end{aligned} \tag{19}$$

where $f(E)$, $g(E)$, $\sigma_{\mathrm{SP/MP}}(E)$, $v(E)$ are the carrier DF obtained for certain device topology and stress conditions, the density-of-states (DOS), Keldysh-like reaction cross section for the SP/MP-processes $\sigma_{\mathrm{SP/MP}} = \sigma_{0,\mathrm{SP/MP}}(E - E_{\mathrm{th,SP/MP}})^{\mathrm{p_{it}}}$ ($\sigma_{0,\mathrm{SP/MP}}$ is the attempt rate and $p_{\mathrm{it}} = 11$) and carrier velocity [25, 30, 31]. $E_{\mathrm{th}} = 1.5$ eV for both processes. Since the AI defines the interface state generation rates, this factor also defines the evolution of interface state density profiles $N_{\mathrm{it}}(x)$ with time. These profiles with the information about trap density-of-states (DOS) are used as input data for MINIMOS-NT. MINIMOS-NT performs device simulations considering the distortion of the device electrostatics and the additional scattering events induced by charged traps. Furthermore, it calculates the device characteristics (output and transfer characteristics, G_{m}, V_{th}, etc.) of the degraded transistor. The feedback to calibrate the model is given by comparison with the experimental device characteristics, Fig. 11.

For the SP-process, I_{SP} directly enters the interface state generation rate, i.e. $\lambda_{\mathrm{SP}} = \nu_{\mathrm{SP}} I_{\mathrm{SP}}$ with ν_{SP} being the attempt rate. Treating the interface state generation as a

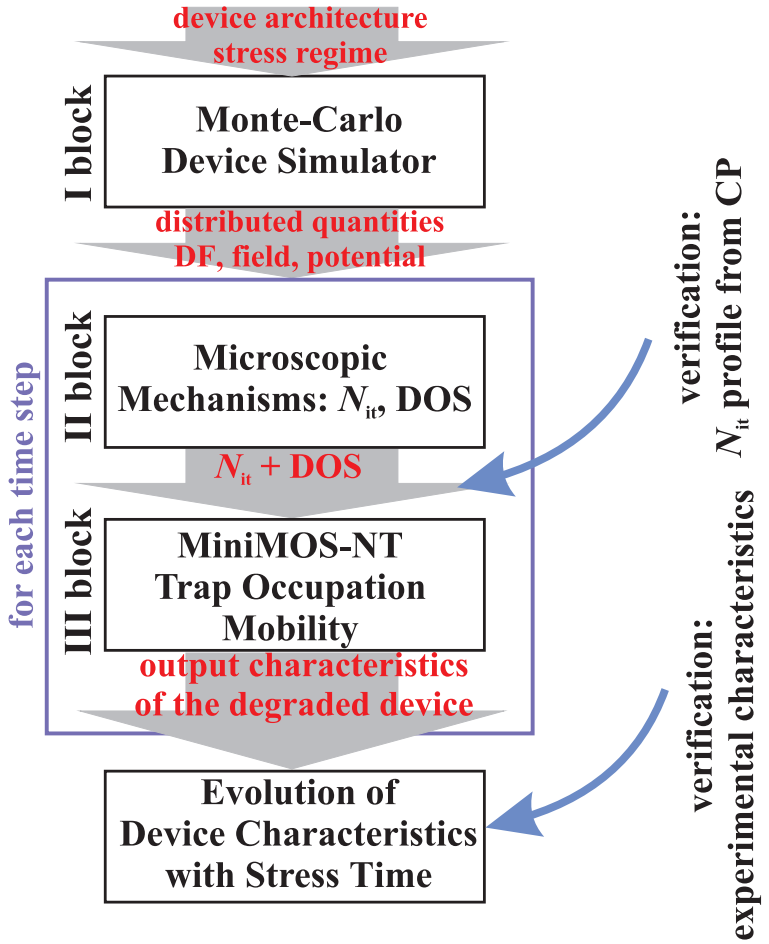

Figure 11: The flowchart of our model for hot-carrier degradation depicting three main modules: carrier transport module, module for microscopic mechanisms for defect creation and module for simulations of degraded devices.

first-order chemical reaction we write:

$$N_{\mathrm{SP}} = N_0 \left(1 - \mathrm{e}^{-\lambda_{\mathrm{SP}} t}\right) \tag{20}$$

As for the MP-process, to describe the kinetics of the oscillator we employ a system of equations similar to those used by Bravaix (cf. with 10). However, in our version of the rate equation system we keep the four terms for the last bonded state N_{l}, that is consider the bond passivation and exchange with the $N_{\mathrm{l}} - 1$ level:

$$\begin{aligned}
\frac{\mathrm{d}n_0}{\mathrm{d}t} &= P_{\mathrm{d}} n_1 - P_{\mathrm{u}} n_0 \\
\frac{\mathrm{d}n_{\mathrm{i}}}{\mathrm{d}t} &= P_{\mathrm{d}}(n_{\mathrm{i}+1} - n_{\mathrm{i}}) - P_{\mathrm{u}}(n_{\mathrm{i}} - n_{\mathrm{i}-1}) \\
\frac{\mathrm{d}n_{N_{\mathrm{l}}}}{\mathrm{d}t} &= P_{\mathrm{u}} n_{N_{\mathrm{l}}-1} - P_{\mathrm{d}} n_{N_{\mathrm{l}}} - P_{\mathrm{emi}} n_{N_{\mathrm{l}}} + \widetilde{P}_{\mathrm{pass}} N_{\mathrm{MP}}^2,
\end{aligned} \tag{21}$$

where to satisfy the dimensionality we use $\widetilde{P}_{\mathrm{pass}} = P_{\mathrm{pass}}/N_0$. This system of rate equations is solved taking into account the time scale hierarchy. The steady-state of the oscillator is established practically momentary as compared to the hydrogen exchange between

the highest bonded and the transport state. Therefore, first the sub-task describing the steady-state of the oscillator is solved recurrently, which results in the following relation between the occupancies of the different levels: $n_{\rm i}/n_0 = (P_{\rm u}/P_{\rm d})^{\rm i}$. Then, the passivation/depassivation rates are considered and the solution of the system (21) is written as:

$$N_{\rm MP} = N_0 \left(\frac{\lambda_{\rm emi}}{P_{\rm pass}} \left(\frac{P_{\rm u}}{P_{\rm d}} \right)^{N_{\rm l}} \left(1 - {\rm e}^{\lambda_{\rm MP} t} \right) \right)^{1/2} . \qquad (22)$$

Note that for weak stresses and/or short stress times ($\lambda_{\rm emi} t \ll 1$) this expression transforms to the root time dependence of (14) and in general has a similar structure. While considering the total concentration of the interface states one should take into account the competing nature of SP- and MP-modes and weight their contributions with certain probabilities, i.e. $N_{\rm it} = p_{\rm SP} N_{\rm SP} + p_{\rm MP} N_{\rm MP}$.

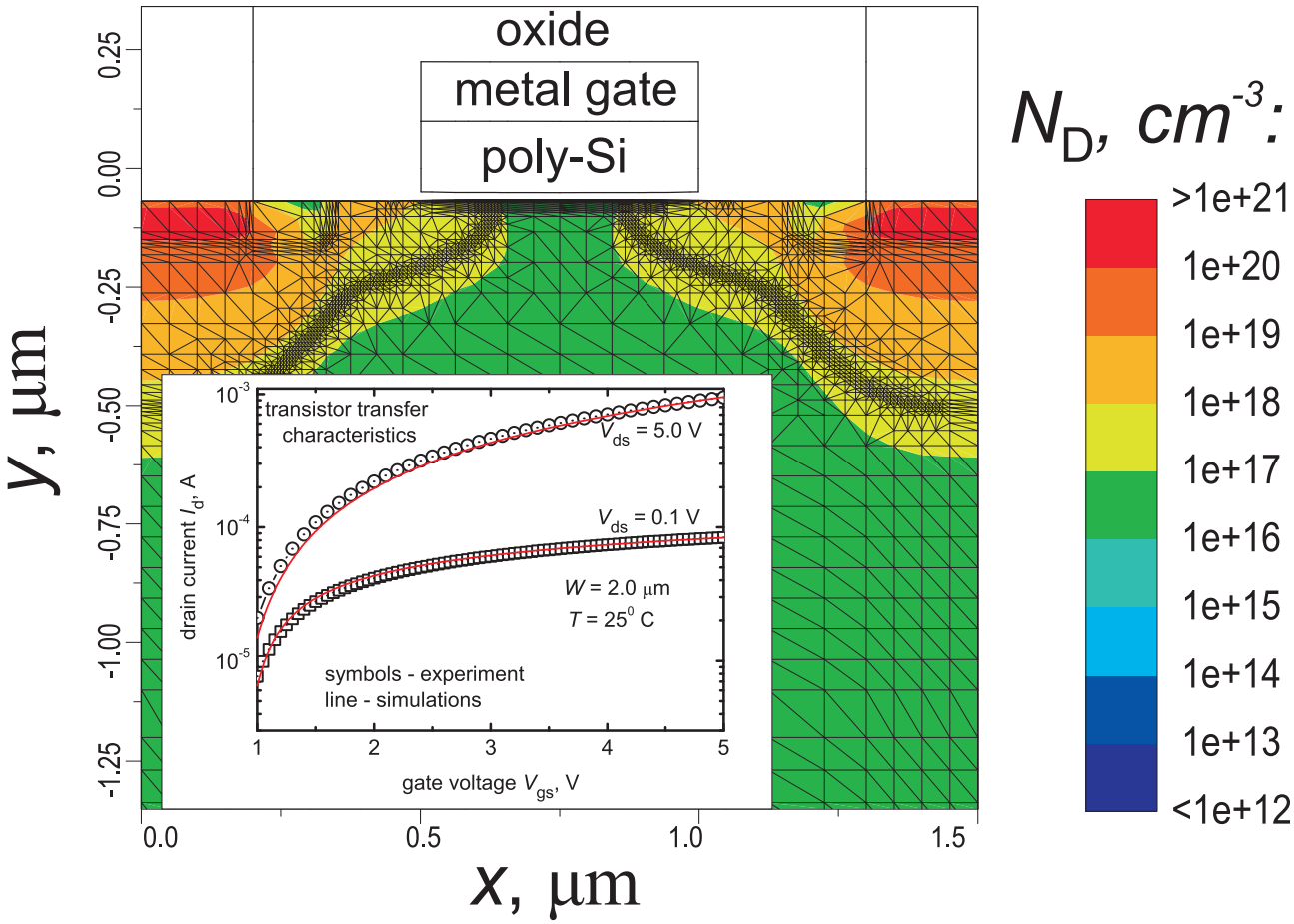

Figure 12: Schematic representation of a 5V n-MOSFETs subjected to hot-carrier stress. Inset: the transfer characteristics of a fresh device represented by our device simulator MINIMOS-NT.

Only charged interface states contribute to the device performance degradation. Therefore, while modeling the transfer characteristic evolution during the hot-carrier stress one should consider effective charges stored in the interface states, not the total concentration

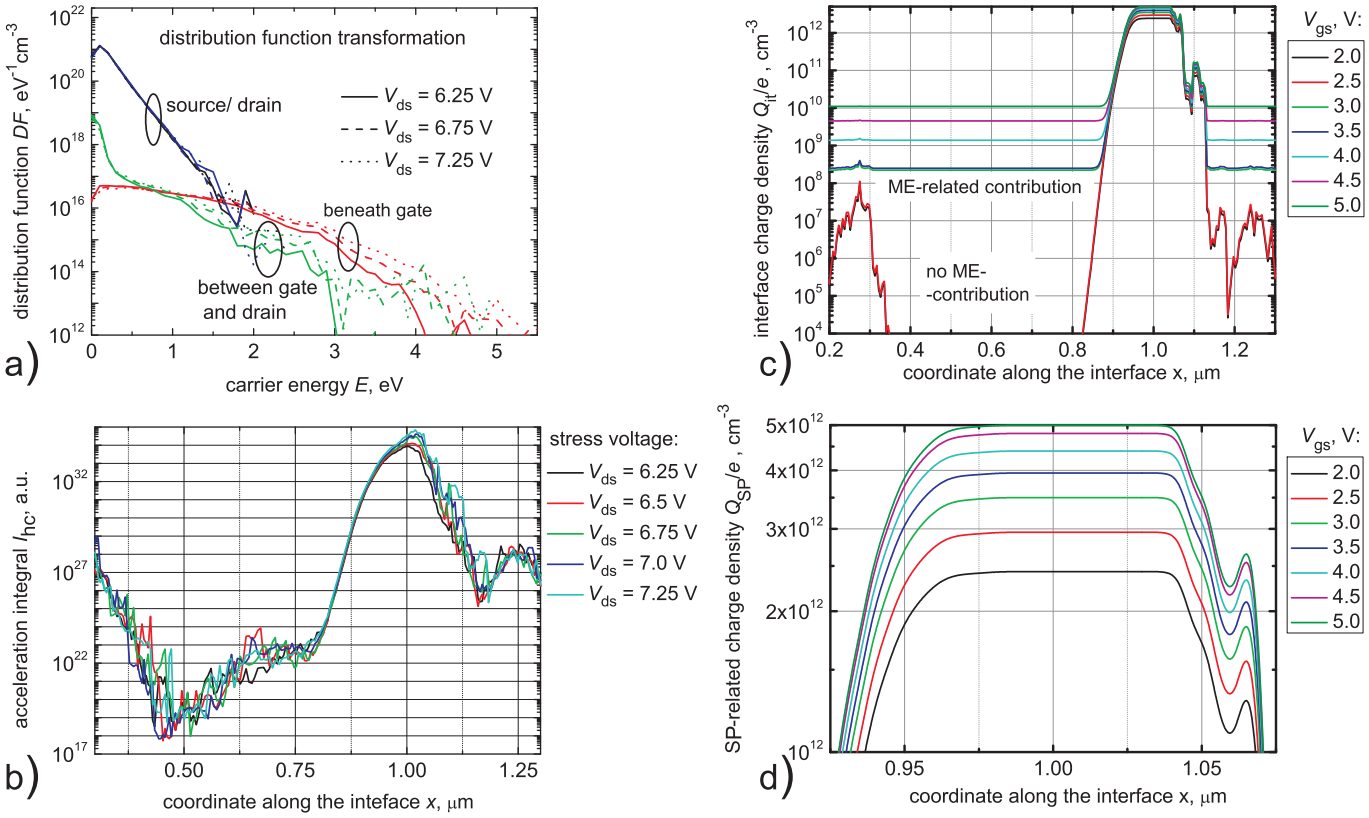

Figure 13: Evolution of crucial characteristics of the degradation with the lateral coordinate: (a) carrier distribution function along the interface; (b) the carrier acceleration integral featuring a peak near the position of most prolonged high-energy tails of the DF; (c) the total interface charge density $Q_{\rm it}$ and (d) stored on the SP-related traps $Q_{\rm MP}$ in the region where the AI peaks.

$N_{\rm it}$. These effective charges ($Q_{\rm SP}$ and $Q_{\rm MP}$, the total $Q_{\rm it}$ is their sum) are defined as:

$$Q_{\rm SP/MP} = \int_{-\infty}^{\infty} g_{\rm SP/MP}(E) f_{\rm oc}(E, E_{\rm F_n}(x)) {\rm d}E, \tag{23}$$

where $g_{\rm SP}(g_{\rm MP})$ are the DOS for the SP(ME)-related traps and $f_{\rm oc}$ is the carrier distribution function obtained for device operation conditions. The coordinate-dependent position of the quasi-Fermi level of electrons is designated as $E_{\rm F_n}$. Note that the functions $g_{\rm SP}$ and $g_{\rm MP}$ are coordinate dependent because of the normalization conditions, i.e. $\int_{-\infty}^{\infty} g_{\rm SP/MP}(E, x){\rm d}E = N_{\rm SP/MP}(x)$. The lateral coordinate also enters the DF for operation conditions because the quasi-Fermi level for carriers captured by traps is position dependent as well. The model is thus calibrated in order to represent the degradation of the linear drain current $I_{\rm dlin}$ over a wide range of stress and/or operation conditions by proper determination of ($Q_{\rm SP}$ and $Q_{\rm MP}$).

For the evaluation of the model we used a high voltage 5V n-MOSFETs fabricated on a standard 0.35 μm technology shown in Fig. 12. Fig. 13a demonstrates the evolution of the carrier distribution function along the channel. One can see that near the source and drain the DF behaves like a heated Maxwellian but has deep high energy-tails at

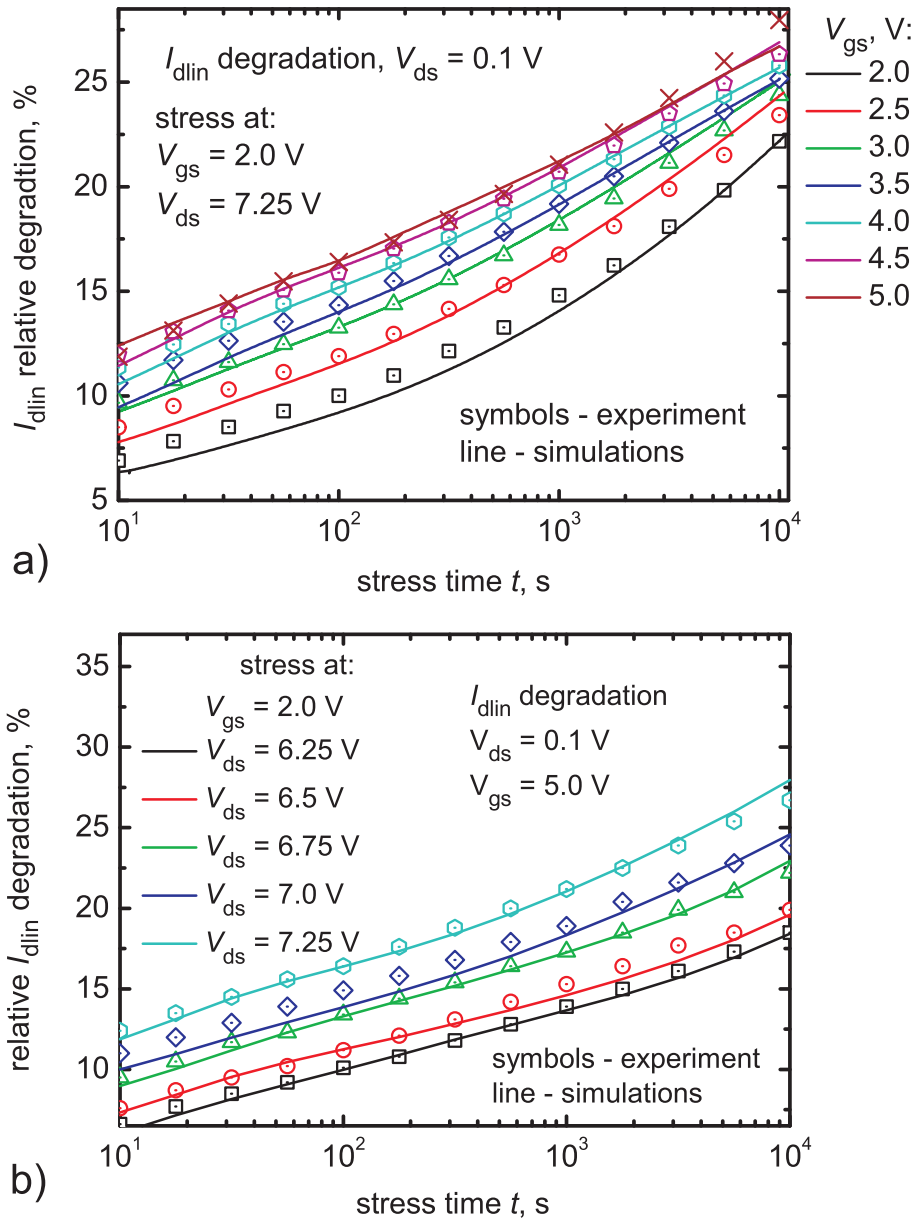

Figure 14: I_{dlin} degradation for different operation V_{gs} and fixed stress conditions $V_{\mathrm{gs}} = 2.0\mathrm{V}$, $V_{\mathrm{ds}} = 7.25\mathrm{V}$ (a) and for different stress V_{ds} and fixed operation $V_{\mathrm{ds}} = 0.1\mathrm{V}$, $V_{\mathrm{gs}} = 5.0\mathrm{V}$ (b).

the drain end of the gate. The carrier acceleration integral plotted vs. the coordinate x (Fig. 13b) features its peak near the area with the most extended high-energy tails of the DF. Such a behavior proves that the hot-carrier induced damage is controlled by the carrier AI which is defined by the shape of the DF. The family of the effective $Q_{\mathrm{it}}(x)$ profiles calculated for various operation conditions at a fixed stress time t of 10s is shown in Fig. 13c,d. One can see that MP-induced defects come into play only for $V_{\mathrm{gs}} \geq 3.0\mathrm{V}$ This circumstance means that the SP- and MP-related states are differently distributed over energy with the latter shifted to higher energies. This result agrees with the concept by Hess *et al.* where the double-power law dependence of the degradation was explained by introducing two time slopes for defects created by different processes [25, 40].

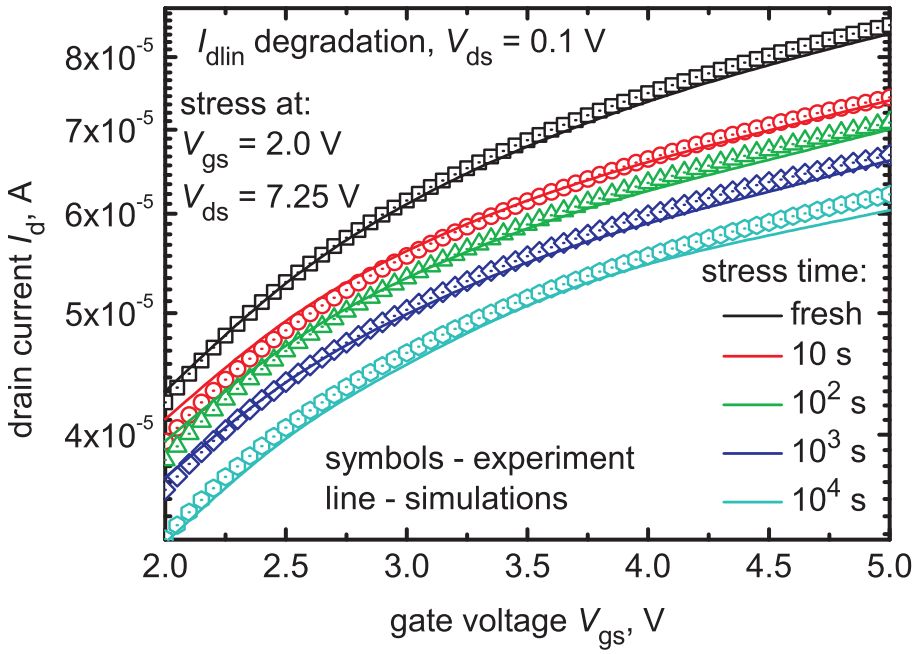

Figure 15: The transformation of the transfer characteristics during the stress: experiment vs. theory.

Fig. 13d resolves the density of particles captured by the SP-traps in the region where the total trap concentration N_{it} is plotted for different V_{gs}. Since out of the N_{it} peak the main contribution to the total density Q_{it} is provided by the MP-process one may compare the behavior of densities related to the different types of traps. For the SP-process the distance between the curves saturates, meaning that interface states of this type are almost fully occupied. In contrast, for the MP-process the increase of charge density continues, indicating that ME-traps are shifted to higher energies.

The model calibrated in the aforementioned manner allows us to represent the I_{dlin} degradation at various V_{gs} (Fig. 14a) and for different stress conditions, i.e. different V_{ds} (Fig. 14b). We do not introduce any additional fitting parameters into the model meaning that N_{it} effectively changes while switching from certain stress conditions to another. Finally, using this approach we are now able to represent the transfer characteristics of the degraded device at each time step, see Fig. 15.

In addition to the interface state generation the bulk oxide charge build-up (with concentration N_{ot}) is another important component often linked in the literature with the hot-carrier stress, which is of special significant in high-voltage devices. In order to check whether this trapped charge considerably contribute to the degradation of device characteristics, we used charge-pumping measurements. In this context, the constant-base-level charge-pumping technique has been employed. Using the approach suggested in [101–103] we were able to resolve the threshold voltage lateral profiles as a function of stress time (Fig. 16.) as well as spatial position of the N_{it} peak which is in good agreement with that obtained from our HCD model (Fig. 17); for the details see [98]. Fig. 16 and its inset representing the threshold voltage shift obtained using the maximal transconductance method show that V_{th} steadily decreases with stress time, however, N_{ot}

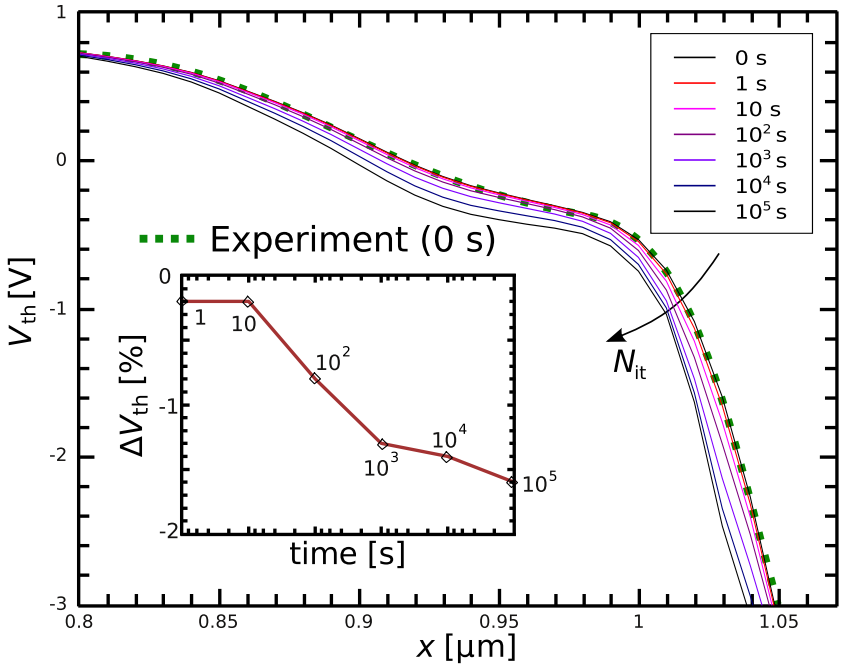

Figure 16: The threshold voltage lateral profile simulated at each time step. Inset: the experimanal change of $V_{\rm th}$ obtained with the maximal transconductance method.

build-up should result in a $V_{\rm th}$ increase or turn-around (when tw o tendencies compensate each other). Another important circumstance confirming that $N_{\rm ot}$ may be neglected is that the charge-pumping current does not shift laterally with the stress time (data not shown).

Some HCD models link the interface state build-up to either the maximum of the electric field, or carrier temperature, or the average electron energy, etc. Fig. 17 provides a short summary showing the spatial positions of the maxima of various quantities which have been used as the driving force of HCD. This information is accompanied by charge-pumping measurements results revealing that the peak of experimental $N_{\rm it}$ coincides with the maximum of the AI (which defines the peak of the simulated $N_{\rm it}$ profile). This tendency confirms once again that the AI is the crucial quantity controlling hot-carrier degradation and just this parameter should primarily been used rather than the electric field or the carrier temperature.

The main advantage of our model is that one does not have to recalibrate it while switching from one device architecture and/or stress conditions to another one(s). In other words, the set of parameters describing the Si-H dissociation kinetics is fitted once and does not depend on process conditions. As for the transport module, the Boltzmann transport equation is to be solved each time we change the device topology and stress conditions to obtain the new set of the DFs corresponding to the current situation. As a result, the model is suitable to predict the device life-time not only for accelerated stress conditions but also under normal operation conditions and thus is useful for development and reliability engineers. Another advantage is that the model provides information about the $N_{\rm it}$ profiles, and in in particular captures the strong localization of HCD. Two additional important peculiarities of hot-carrier degradation captured by the model are the

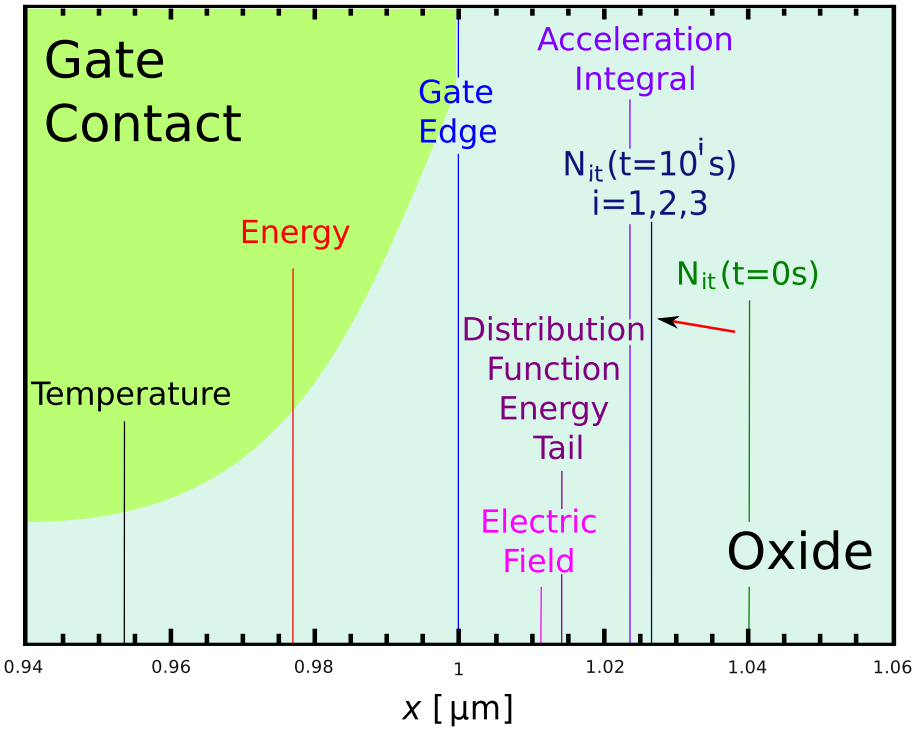

Figure 17: The position of maxima of main crucial quantities: the electric field, average carrier energy, acceleration integral, position of the most extended tails of the, etc.

saturation of the damage as well as the representation of the worst-case conditions [97].

Conclusion

We have carefully analyzed the main approaches to hot-carrier degradation modeling and established a comprehensive framework of a physics-based HCD model. As was demonstrated within the model by Hess, the degradation is controlled by the interplay between single- and multiple-carrier mechanisms of Si-H bond dissociation. This interplay is controlled by the way the carriers are distributed over energy, that is by the carrier energy distribution function. These considerations suggest that carrier transport and microscopic mechanisms of defect creation are two essential sub-tasks of the general problem. While the energy-driven paradigm elaborated by Rauch and LaRosa is focused on the substitution of the DF by some simple approximations, the Bravaix model combines this paradigm with defect generation concepts. After discussion of the advantages and limitations of the models we have introduced our approach based on a thorough evaluation of the carrier DF by solving the Boltzmann transport equation. This concept arranges the whole hierarchical ladder by integrating carrier transport aspects, the microscopic picture of defect creation, and the simulation of degraded devices within the same framework. We have proven that for proper HCD description one should deal with the carrier acceleration integral, not with other factors such as the electric field or average carrier energies.

Acknowledgments

This work has received funding from the EC's FP7 grant agreement n°216436 (ATHENIS) and from the ENIAC MODERN project n°820379.

References

1. A. Acovic, G. L. Rosa, and Y. Sun, *Microel. Reliab.* **36**, 845–869 (1996).
2. S. Rauch, and G. L. Rosa, "CMOS Hot Carrier: From Physics to End Of Life Projections, and Qualification," in *Proc. International Reliability Physics Symposium (IRPS), tutorial*, 2010.
3. A. Bravaix, and V. Huard, "Hot-Carrier Degradation Issues in advanced CMOS nodes," in *Proc. European Symposium on Reliability of Electron Devices Failure Physics and Analysis (ESREF), tutorial*, 2010.
4. Y. Liu, *Study of oxide breakdown, hot carrier and NBTI effect on MOS device and circuit reliability*, Ph.D. thesis, University of Central Florida, Orlando, Florida (2005).
5. G. Groeseneken, R. Bellens, and G. V. den Bosch, *Semicond. Sci. Technol.* **10**, 1208–1220 (1995).
6. C. Hu, "Lucky electron model for channel hot electron emission," in *Proc. International Electron Devices Meeting (IEDM)*, 1979, pp. 22–25.
7. C. Hu, S. Tam, F. Hsu, P.-K. Ko, T.-Y. Chan, and K. Terrill, *IEEE Trans. Electron Dev.* **48**, 375–385 (1985).
8. S. Rauch, F. Guarin, and G. LaRosa, *IEEE Electron Dev. Lett.* **19**, 463–465 (1998).
9. E. Takeda, *IEEE Proc.* **131**, 153–162 (1984).
10. E. Takeda, and N. Suzuki, *IEEE Electron Dev. Lett.* **4**, 111–113 (1983).
11. J.-S. Goo, Y.-G. Kim, H. Lee, H.-Y. Kwon, and H. Shin, *Solid-State Electron.* **38**, 1191–1196 (1995).
12. R. Dreesen, K. Croes, J. Manca, W. D. Ceunick, L. D. Schepper, A. Pergoot, and G. Groeseneken, *Microel. Reliab.* **39**, 785–790 (1999).
13. R. Dreesen, K. Croes, J. Manca, W. D. Ceunick, L. D. Schepper, A. Pergoot, and G. Groeseneken, *Microel. Reliab.* **41**, 437–443 (2001).
14. R. Woltjer, and G. Paulzen, "Universal description of hot-carrier-induced interface states in NMOSFETs," in *Proc. International Electron Devices Meeting (IEDM)*, 1992, pp. 535–538.
15. R. Woltjer, G. Paulzen, H. Pomp, H. Lifka, and P. Woerlee, *IEEE Trans. Electron Dev.* **42**, 109–115 (1995).
16. K. Mistry, and B. Doyle, *IEEE Electron Dev. Lett.* **12**, 492–494 (1991).
17. K. Mistry, and B. Doyle, *IEEE Trans. Electron Dev.* **40**, 96–104 (1993).
18. S. Rauch, G. LaRosa, and F. Guarin, *IEEE Trans Dev. Material. Reliab.* **1**, 113–119 (2001).
19. C. Guerin, V. Huard, and A. Bravaix, *IEEE Trans. Dev. Material. Reliab.* **7**, 225–235 (2007).
20. P. Moens, and G. van den Bosch, *IEEE Trans Electron Dev.* **6**, 349–357 (2006).
21. P. Moens, G. van den Bosch, and G. Groeseneken, "Competing hot carrier degradation mechanisms in lateral n-type DMOS transistors," in *Proc. International Reliability Physics Symposium (IRPS)*, 2003, pp. 214–221.
22. P. Moens, and M. Tack, "Hole trapping and de-trapping effects in LDMOS devices under dynamic stress," in *Proc. International Electron Devices Meeting (IEDM)*, 2006.

23. P. Moens, F. Bauwens, M. Nelson, and M. Tack, "Electron trapping and interface trap generation in drain extended pMOS transistors," in *Proc. International Reliability Physics Symposium (IRPS)*, 2005, pp. 93–96.
24. W. McMahon, A. Haggaag, and K. Hess, *IEEE Trans. Nanotech.* **2**, 33–38 (2003).
25. K. Hess, A. Haggag, W. McMahon, K. Cheng, J. Lee, and J. Lyding, *Circuits and Devices Mag.* pp. 33–38 (2001).
26. O. Penzin, A. Haggag, W. McMahon, E. Lyumkis, and K. Hess, *IEEE Trans. Electron Dev.* **50**, 1445–1450 (2003).
27. H. Kufluoglu, and M. Alam, *Journ. Comput. Electron.* **3**, 165–169 (2004).
28. H. Kufluoglu, *MOSFET degradation due to negative bias temperature instability (NBTI) and hot carrier degradation (HCI) and its applications for reliability-aware VLSI design*, Ph.D. thesis, Purdue University, West Lafayette, Indiana, USA (2007).
29. S. Rauch, and G. L. Rosa, "The Energy Driven Paradigm of NMOSFET Hot Carrier Effects," in *Proc. International Reliability Physics Symposium (IRPS)*, 2005.
30. A. Bravaix, C. Guerin, V. Huard, D. Roy, J. Roux, and E. Vincent, *Proc. IRPS* pp. 531–546 (2009).
31. C. Guerin, V. Huard, and A. Bravaix, *Journ. Appl. Phys.* **105** (2009).
32. W. McMahon, K. Matsuda, J. Lee, K. Hess, and J. Lyding, "The Effects of a multiple carrier model of interface states generation of lifetime extraction for MOSFETs," in *Proc. Int. Conf. Mod. Sim. Micro*, 2002, vol. 1, pp. 576–579.
33. K. Hess, I. C. Kizilyalli, and J. W. Lyding, *IEEE Trans Electron Dev.* **45**, 406–416 (1998).
34. T. Grasser, W. Gös, and B. Kaczer, *ECS Transactions* **19**, 265–287 (2009).
35. W. Chang, B. Davari, M. Wordeman, Y. Taur, C. Hsu, and M. Rodriguez, *IEEE Trans. Electron Dev.* **39**, 959 (1992).
36. D. Bursky, *Electronic Design* **41**, 111–116 (1993).
37. D. Frank, R. Dennard, E. Nowak, P. Solomon, M. Stettler, S. Tyagi, and M. Bohr, "Scaling challenges and device design requirements for high performance sub-50 nm gate length planar CMOS transistors," in *Proc. VLSI Symposium Tech. Digest*, 2000, pp. 174–175.
38. L. Hong, *Characterization of hot carrier reliability in deep submicrometer MOSFETsL. Hong*, Ph.D. thesis, National University of Singapore (2005).
39. F.-C. Hsu, and K.-Y. Chu, *IEEE Electron Dev. Lett.* **5**, 162–165 (1984).
40. A. Haggag, W. McMahon, K. Hess, K. Cheng, J. Lee, and J. Lyding, "High-performance chip reliability from short-time-tests. Statistical models for optical interconnect and HCI/TDDB/NBTI deep-submicron transistor failures," in *Proc. International Reliability Physics Symposium (IRPS)*, 2001, pp. 271–279.
41. T. Mizuno, A. Toriumi, M. Iwase, M. Takanashi, H. Niiyama, M. Fukmoto, and M. Yoshimi, "Hot-carrier effects in 0.1 μm gate length CMOS devices," in *Proc. International Electron Devices Meeting (IEDM)*, 1992, pp. 695–698.
42. J. Bude, "Gate-Current by Impact Ionization Feedback in submicron MOSFET Technologies," in *Proc. VLSI Symposium Tech. Digest*, 1995, pp. 101–102.
43. F. Venturi, E. Sangiorgi, and B. Ricco, *IEEE Trans. Electron Dev.* **38**, 1895–1904 (1991).
44. J. Chung, M. Jeng, J. Moon, P. Ko, and C. Hu, *IEEE Trans. Electron Dev.* **37**, 1651–1657 (1990).
45. M. Fischetti, and S. Laux, "Monte-Carlo study of sub-band-gap impact ionization in

small silicon field-effect transistors," in *Proc. International Electron Devices Meeting (IEDM)*, 1995, pp. 305–308.
46. S. Tyaginov, I. Starkov, O. Triebl, J. Cervenka, C. Jungemann, S. Carniello, J. Park, H. Enichlmair, M. Karner, C. Kernstock, E. Seebacher, R. Minixhofer, H. Ceric, and T. Grasser, "Hot-Carrier Degradation Modeling Using Full-Band Monte-Carlo Simulations," in *Proc. International Symposium on the Physical & Failure Analysis of Integrated Circuits (IPFA)*, 2010.
47. S. Tyaginov, I. Starkov, O. Triebl, J. Cervenka, C. Jungemann, S. Carniello, J. Park, H. Enichlmail, C. Kernstock, E. Seebacher, R. Minixhofer, H. Ceric, and T. Grasser, *Microel. Reliab.* **50**, 1267–1272 (2010).
48. D. Brisbin, P. Lindorfer, and P. Chaparala, "Substrate current independent hot carrier degradation in NLDMOS devices," in *Proc. International Reliability Physics Symposium (IRPS)*, 2006, pp. 329–333.
49. M. Annese, S. Carniello, and S.Manzini, *IEEE Trans. Electron Dev.* **52**, 1634–1639 (2005).
50. P. Santos, H. Quaresma, A. Silva, and M. Lanca, *Microel. Jour.* **35**, 723–730 (2004).
51. W. Qin, W. Chim, D. H. Chan, and C. Lou, *Semicond. Sci. Technol.* **13**, 453–459 (1998).
52. S. Manzini, and A. Gallerano, *Solid-State Electron.* **44**, 1325–1330 (2000).
53. V. Reddy, "An introduction to CMOS semiconductor reliability," in *Proc. International Reliability Physics Symposium (IRPS), tutorial*, 2003.
54. Z. Chen, P. Ong, A. Mylin, V. Singh, and S. Cheltur, *Appl. Phys. Lett.* **81**, 3278–3280 (2002).
55. E. Li, E. Rosenbaum, J. Tao, G.-F. Yeap, M. Lin, and P. Fang, "Hot-carrier effects in nMOSFETs in 0.1 μm CMOS technology," in *Proc. International Reliability Physics Symposium (IRPS)*, 1999, pp. 253–258.
56. C. Lin, S. Biesemans, L. Han, K. Houlihan, T. Schiml, K. Schruefer, C. Wann, and R. Markhopf, "Hot carrier reliability for 0.13 μm CMOS technology with dual gate oxide thickness," in *Proc. International Electron Devices Meeting (IEDM)*, 2000, pp. 135–138.
57. R. Woltjer, A. Hamada, and E. Takeda, *Semicond Sci. Technol.* **7**, pp. B581–B584 (1992).
58. A. Bravaix, D. Goguenheim, N. Revil, and E. Vincent, *Microel. Reliab.* **44**, 65–77 (2004).
59. M. Ancona, N. Saks, and D. McCarthy, *IEEE Trans Electron Dev.* **35**, 221–2228 (1988).
60. M. Pagey, *Characterization and modeling of hot-carrier degradation in sub-micron NMOSFETs*, Master's thesis, Vanderbilt University (2002).
61. Q. Wang, L. Sun, and A. Yap, *Microel. Reliab.* pp. 508–513 (2008).
62. Q. Wang, L. Sun, Z. Zhang, A. Yap, H. Li, and S. Liu, *Journ. Non-Crystalline Solids* **354**, 1871–1875 (2008).
63. K.-M. Wu, J. Chen, Y. Su, J. Lee, K. Lin, J. Shih, and S. Hsu, *Appl. Phys. Lett.* **89** (2006).
64. T. Grasser, H. Kosina, and S. Selberherr, *Journ. Appl. Phys.* **90**, 6165–6171 (2001).
65. A. Gehring, T. Grasser, H. Kosina, and S. Selberherr, *Journal of Applied Physics* **92**, 6019–6027 (2002).
66. T. Grasser, H. Kosina, and S. Selberherr, *International Journal of High Speed Elec-*

tronics and Systems **13**, 873–901 (2003).
67. A. Zaka, Q. Rafhay, M. Iellina, P. Palestri, R. Clerc, D. Rideau, D. Garetto, J. Singer, G. Pananakakis, C. Tavernier, and H. Jaouen, *Solid-State Electron.* **in press** (2010).
68. B. Persson, and P. Avouris, *Surface Science* **390**, 45–54 (1997).
69. K. Hess, L. Register, B. Tuttle, J. Lyding, and I. Kizilyalli, *Physica E* **3**, 1–7 (1998).
70. T. Aichinger, M. Nelhiebel, and T. Grasser, *Microel. Reliab.* pp. 1178–1184 (2008).
71. T. Grasser, B. Kaczer, W. Goes, H. Reisinger, T. Aichinger, P. Hehenberger, P.-J. Wagner, F. Schanowsky, J. Franco, P. Roussel, and M. Nelhiebel, "Recent Advances in Understanding the Bias Temperature Instability," in *Proc. International Electron Devices Meeting (IEDM)*, 2010, pp. 82–85.
72. F.-C. Hsu, and K.-Y. Chu, *IEEE Electron Dev. Lett.* **5**, 148–150 (1984).
73. P. Heremans, G. V. den Bosch, R. Bellens, G. Groseneken, and H. Maes, *IEEE Trans. Electron Dev.* **37**, 980–992 (1990).
74. M. Song, K. MacWilliams, and C. Woo, *IEEE Trans Electron Dev.* **44**, 268–276 (1997).
75. A. Bravaix, D. Goguenheim, N. Revil, E. Vincent, M. Varrot, and P. Mortini, *Microel. Reliab.* **39**, 35–44 (1999).
76. P. Moens, J. Mertens, F. bauwens, P. Joris, W. D. Ceuninck, and M. Tack, "A comprehensive model for hot carrier degradation in LDMOS transistors," in *Proc. International Reliability Physics Symposium (IRPS)*, 2007, pp. 492–497.
77. H. Enichlmair, S. Carniello, J. Park, and R. Minixhofer, *Microel. Reliab.* **47**, 1439–1443 (2007).
78. K. Lee, C. Kang, O. yoo, R. Choi, B. Lee, J. Lee, H.-D. Lee, and Y.-H. Jeong, *IEEE Electron Dev. Lett.* **29**, 389–391 (2008).
79. M. Jo, S. Kim, C. Cho, M. Chang, and H. Hwang, *Appl. Phys. Lett.* **94**, 053505–1–053505–3 (2009).
80. E. Amat, T. Kauerauf, R. Degraeve, R. Rodriguez, M. Nafria, X. Aymerich, and G. Groeseneken, *Microel. Engineering* **87**, 47–50 (2010).
81. R. Walkup, D. Newns, and P. Avouris, *Phys. Rev. B* **48**, 1858–1861 (1993).
82. J. Lyding, K. Hess, G. Abeln, D. Thompson, J. Moore, M. Hersam, E. Foley, J. Lee, S. Hwang, H. Choi, P. Avouris, and I. Kizialli, *Appl. Surf. Sci.* **13-132**, 221–230 (1998).
83. K. Stokbro, C. Thirstrup, M. Sakurai, U. Quaade, B. Y.-K. Hu, F. Perez-Murano, and F. Grey, *Phys. Rev. Lett.* **80**, 2618–2621 (1998).
84. M. Budde, G. Lüpke, E. Chen, X. Zhang, N. H. Tolk, L. C. Feldman, E. Tarhan, A. K. Ramdas, and M. Stavola, *Phys. Rev. Lett.* **87**, 1455–1461 (2001).
85. J. Sune, and Y. Wu, *Phys. Rev. Lett.* **92**, 087601 (1–4) (2004).
86. J. Sune, and Y. Wu, "Mechanisms of hydrogen release in the breakdown of SiO_2-based oxides," in *Proc. International Electron Devices Meeting (IEDM)*, 2005, pp. 388–391.
87. R. Biswas, Y.-P. Li, and B. C. Pan, *Appl. Phys. Lett.* **72**, 3500–3503 (1998).
88. G. Ribes, S. Bruyere, M. Denais, F. Monsieur, V. Huard, D. Roy, and G. Ghibaudo, *Microel. Reliab.* **45**, 1842–1854 (2005).
89. B. Tuttle, and C. V. de Walle, *Phys. Rev. B* **59**, 12884–12889 (1999).
90. K. Hess, A. Haggag, W. McMahon, B. Fischer, K. Cheng, J. Lee, and L. Lyding, "Simulation of Si-SiO2 Defect Generation in CMOS Chips: From Atomistic Structure to Chip Failure Rates," in *Proc. International Electron Devices Meeting*

(IEDM), 2000, pp. 93–96.
91. *DESSIS manual*.
92. H. Kufluoglu, and M. Alam, "A geometrical unification of the theories of NBTI and HCI time exponents and its implications for ultra-scaled planar and surround-gate MOSFETs," in *Proc. International Electron Devices Meeting (IEDM)*, 2004, pp. 113–116.
93. T.Grasser, W. Gös, and B. Kaczer, *IEEE Trans Dev. Material. Reliab.* **8**, 79–97 (2008).
94. T. Grasser, H. Reisinger, W. Goes, T. Aichinger, P. Hehenberger, P.-J. Wagner, M. Nelhiebel, J. Franco, and B. Kaczer, "Switching Oxide Traps as the Missing Link Between Negative Bias Temperature Instability and Random Telegraph Noise," in *Proc. International Electron Devices Meeting (IEDM)*, 2009.
95. T. Grasser, H. Reisinger, P.-J. Wagner, D. Kaczer, F. Schanowsky, and W. Gös, "The time dependent defect spectroscopy (TDDS) for the characterization of the bias temperature instability," in *Proc. International Reliability Physics Symposium (IRPS)*, 2010, pp. 16–25.
96. S. Rauch, and G. L. R. and, *IEEE Trans Dev. Material. Reliab.* **5**, 701–705 (2005).
97. I. Starkov, S. Tyaginov, O. Triebl, J. Cervenka, C. Jungemann, J. Park, H. Enichlmair, M. Karner, C. Kernstock, E. Seebacher, R. Minixhofer, H. Ceric, and T. Grasser, "Analysis of Worst-Case Hot-Carrier Conditions for High Voltage Transistors Based on Monte-Carlo Simulations of Distribution Function," in *Proc. International Symposium on the Physical & Failure Analysis of Integrated Circuits (IPFA)*, 2010.
98. I. Starkov, S. Tyaginov, H. Enichlmair, J. Cervenka, C. Jungemann, S. Carniello, J. Park, H. Ceric, and T. Grasser, *Journal of Vacuum Science and Technology - B* **in press** (2010).
99. C. Jungemann, and B. Meinerzhagen, *Hierarchical Device Simulation*, Springer Verlag Wien/New York, 2003.
100. Institute for Microelectronic, TU Wien, *MiniMOS-NT Device and Circuit Simulator*.
101. C. Chen, and T. Ma, *IEEE Trans Electron Dev.* **45**, 512–520 (1998).
102. S. Chung, and J.-J. Yang, *IEEE Trans Electron Dev.* **46**, 1371–1377 (1999).
103. Y.-L. Chu, D.-W. Lin, and C.-Y. Wu, *IEEE Trans. Electron Dev.* **47**, 348–353 (2000).